Next Materials 3 (2024) 100192

Contents lists available at ScienceDirect

Next Materials

journal homepage: www.sciencedirect.com/journal/next-materials

Review article

High entropy oxides: New superior supports for single atom catalysts

Panesun Tukur [a], Frank Tukur [a], Yirong Mo [a], Qiangu Yan [b], Chaochao Dun [c], Jianjun Wei [a,*]

[a] The Department of Nanoscience, Joint School of Nanoscience and Nanoengineering, University of North Carolina at Greensboro, 2709 E Gate City Blvd, Greensboro, NC 27401, USA
[b] USDA Forest Products Laboratory, Madison, WI 53726, USA
[c] The Molecular Foundry, Lawrence Berkeley National Laboratory One Cyclotron Road, Building 67, Berkeley, CA 94720, USA

ARTICLE INFO

Keywords:
Single atom catalyst
High entropy oxide supports
Heterogenous catalyst
Stability and activity
Synthetic approach
Single-phase formation

ABSTRACT

Single Atom catalyst (SAC), a new frontier in heterogeneous catalyst design has evolved as a novel strategy to resolve the cost puzzle hindering the commercial scale applications of benchmark noble metal catalysts in various technologies. Downsizing expensive noble metal catalyst to atomically active centers have simultaneously reduced cost via enhanced atom utilization and maximized their catalytic activity and selectivity. However, taking full advantages of this novelty requires stabilization on appropriate support materials that provide adequate anchoring sites, promote strong metal support-interaction, ensure adequate stabilities to withstand extreme chemical or thermal reaction conditions, and favorably modulate their electronic structures for optimal performance. High entropy oxides (HEOs), characterized by unusual synergistic effects, highly reducible surface lattice oxygen, and high thermal and chemical stabilities, have recently emerged as a new type of support for SACs with superior performances. Despite their immense potential to reinvent the heterogenous catalyst design, single atoms supported on HEOs have not received adequate attention. Herein fundamental aspects regarding HEOs such as their discovery, design rules, stabilization criteria, computater aided design, and emerging synthesis approaches suitable for catalytic applications have been presented in this review. We also provide a detailed perspective of the SACs/HEO domains, highlighting their synthesis, entropy-driven properties, catalytic performance, and stabilities during thermochemical processes at elevated temperatures. Although high entropy materials have been highlighted in a few recent reviews, this review is the first strictly exclusive to single atoms supported on HEOs.

1. Introduction

Depletion of fossil-based energy sources and environmental pollution accompanying their usage are two major motivations behind the resilient interest in developing clean energy conversion and storage technologies [1–3]. Based on the Representative Concentration Pathways (RCP8.5 under the business-as-usual scenario) projections, end-of-century CO_2 emission is expected to reach 105.6 Gt/year with a resultant average global temperature rise of 4.5 °C [4]. This increase in temperature holds a great potential for substantial deleterious effects across all sectors of the United States economy as only 1 °C increase in average global temperature is associated with 1.2% decrease in Gross domestic product (GDP), with an anticipated decrease in agricultural yields by 9.1%, increase property crime by 0.88%, energy demand rises by 5.4%, mortality rates increase by 5.4% for every 100,000 deaths, 0.11% and 0.53% decline in total labor hours for low and high-risk workers respectively in the United States [5]. If not mitigated, this escalating warming trend could result in a 23% decrease in average global income by the end of the century, further exacerbating global income inequality. The adverse effect of this climate change has demonstrated an unusual distribution pattern with developing nations in the global south experiencing more severe repercussions compared to the more industrialized countries which contribute more to the global CO_2 emission [6]. This emphasizes the urgent need for collective action

Abbreviations: SACs, Single-atom catalysts; HEOs, high entropy oxides; MSI, metal-support interaction; MEO, multi-element oxides; XRD, X-ray diffraction; STEM, Scanning transmission electron microscopy; EDS, energy dispersive spectroscopy; EXAFS, Extended X-ray absorption fine structure; XANES, X-ray adsorption near edge spectroscopy; DFT, Density functional theory; HAADF, High angular annular dark field; XPS, X-ray photoelectron spectroscopy; HEFO, high entropy fluorite oxide; HEPOs, high entropy perovskite oxides; ESO, entropy stabilized oxides; HEA, high entropy alloy; VEC, valence electron concentration; NP, nanoparticles.

* Corresponding author.
E-mail address: j_wei@uncg.edu (J. Wei).

https://doi.org/10.1016/j.nxmate.2024.100192
Received 3 February 2024; Received in revised form 20 March 2024; Accepted 28 March 2024
Available online 3 April 2024

to reduce CO_2 emissions in all sectors and locations.

A long-standing strategy for decarbonization has been the application of energy harvesting and storage technologies to electrify the energy sector. These technologies rely on various chemical transformations that require energy input in the form of heat, light, or electrical potential [2,3,7–9]. This makes catalysts highly indispensable for minimizing such energy barriers while maximizing speed and selectivity towards the desired reactions [9–17], Hence, there has been a growing interest in developing highly efficient catalyst systems tailored to specific chemical reactions [8,18–20].

Generally, catalysts can be categorized as homogenous or heterogenous, depending on the catalyst phase relative to the reactants. Catalysts are regarded as homogenous when the catalyst, reactants, and sometimes the products are in the same phase [21]. These catalysts feature metal active centres stabilized by coordinating with ligands. The well-defined active sites and flexible coordination environment in the catalysts make them highly active and selective for a specific reaction. Such activity and selectivity could be enhanced by modulating the metal active centres or their coordination environments [22,23]. Despite their high reactivity and selectivity, industrial scale applications of homogenous catalysts are hindered due to poor stabilities and extreme difficulty to recover at the end of the reactions [24]. On the other hand, heterogeneous catalysts feature metals or ionic compounds which could directly serve as catalysts or as supports for clusters or nanoparticles (NPs) [25]. Because such catalysts exist in different phase from the reactants, they are easily recovered at the end of the reaction. Also, heterogenous catalysts are relatively stable under harsh chemical or thermal environments thus are desirable for industrial scale applications [25]. Heterogeneous catalytic reactions occur at the interface between the solid catalyst surface and the reactants, where the exposed surface atoms play a crucial role in catalytic activity [25,26]. Therefore, the amount of exposed surface atoms becomes particularly important to the catalytic activity [27]. The size of particles is associated with the exposed surface atoms [28] and the electronic state [29] thus is strongly correlated to its resultant catalytic activity and selectivity [30]. Smaller-sized catalyst particles with a higher proportion of exposed surface atoms exhibit improved catalytic activity and selectivity, making downsizing the catalyst a promising approach [31].

Stabilizing isolated metal atoms on suitable substrates has emerged as an effective strategy to create highly active and selective catalysts for various important chemical transformations [15,32]. This approach, first introduced by Zhang et al. for CO oxidation, aims to reduce metal catalysts to atomically active units, increasing atom utilization and reducing costs, particularly for rare and expensive noble metals [33]. The superior performance of these catalyst systems has led to extensive research efforts to stabilize single atoms of main group, transition metals, and noble metals on suitable support materials [3,10,11,13, 32–38]. Many such catalyst systems have been synthesized and explored for thermocatalytic, electrocatalytic, and photocatalytic processes, and their exceptional performance results from their unique geometric features and electronic structures [31]. Stabilizing mononuclear metal active centres on suitable substrates has effectively bridged the gap between homogeneous and heterogeneous catalysts [1,33,38-41], leading to the development of single-atom catalysts (SACs) [45]. SACs have attracted attention due to their superior catalytic activity and selectivity, with recent advances in atomically resolved characterization and computational techniques providing insights into their structure-activity relationships and reaction mechanisms.

The increased atom utilization and construction of unique geometric and electronic sites that arise from stabilizing mononuclear metal active centres on suitable substrates have significantly bridged the gap between homogenous and heterogeneous catalysts [1,33,39-41]. Such catalyst design, popularly regarded as SACs featuring an isolated metal M_1 on substrates represented by M_1/Support (e.g., Pt_1/FeO_x), has significantly attracted attention due to their superior catalytic activity and selectivity. Recent advances in atomically resolved characterization and computational techniques have allowed for a deeper probing of the structure-activity relationships as well as elucidation of reaction mechanisms at various active centres. Such information is particularly beneficial towards the rational construction of strong coordination bonds that ensure strong covalent or ionic interactions between the metal centres and the support. This is particularly important as metal-support interaction significantly affects the catalytic performance and stability [17,39,42]. Therefore, careful selection of appropriate support materials becomes increasingly important. Fig. 1 below illustrates the motivation for the exploration of SACs, which stems from the fundamental limitations associated with heterogenous and homogenous catalysts.

Unfortunately, leaching of metal active sites in SACs due to unstable metal-support bonding and low metal loadings affects the space-time yields of SACs, while high loadings may lead to sintering or aggregation [39]. Therefore, recent design strategies have focused on achieving SACs with higher stability against sintering while featuring dense and uniform distribution of active sites with tailored electronic configuration [11] or geometric structures by local coordination [21] for targeted applications. To achieve the goals, the synthetic techniques and types of support need to be carefully optimized respectively. To date, several synthetic techniques have been used to stabilize SACs on different materials with various underlying geometries and chemistries as extensively discussed in these recommended review articles [1,41]. For example, partially oxidized single nickel atoms stabilized on polymeric carbon nitride demonstrate remarkable activity and selectivity toward photocatalytic hydrogen evolution reaction [11]. Similarly, single Cu atoms stabilized on TiO_2 supports exhibit high photocatalytic hydrogen gas production with a quantum efficiency of 56% [43]. Oxides of reducible metals such as Fe_2O_3, CeO_2, and Al_2O_3 have been shown to stabilize single metal (M) centres by bonding to oxygen atoms of the support to form an M-O_n motif (n=2–4) [25,41]. Experimental and theoretical studies have established carbon materials doped with heteroatoms such as N or S as good anchoring sites for single metal atoms. The single metals are stabilized through the formation of M-N-C or M-S-C bonds. In addition, the basic chemistry of other materials, such as graphene, metals, metal-organic frameworks (MOFs) etc., have been explored to stabilize the single atom metal centres [17].

HEO systems which leverage high configurational entropy to stabilize up to five different cations in the same sub-lattice have currently evolved as robust multi-metallic catalyst systems. The immense compositional and structural tunability of metal active sites [44] with highly reducible lattice and surface oxygen species [45] makes HEOs highly suitable for catalytic applications. Fundamentally, oxygen vacancies, M-O bonds, and metal centres in HEOs can serve as active sites for various catalytic transformations. Furthermore, entropic stabilization affords these materials with high thermal and chemical stabilities which make them useful as supports for different catalyst systems spanning single atoms, clusters, or NPs. Such high thermal and chemical stabilities may therefore be leveraged to prevent sintering problems associated with SACs.

Also, HEOs have demonstrated synthesizability via different methods that could naturally be used to stabilize SACs [41,46]. Therefore, anchoring SACs on HEOs would not require any additional synthetic steps or protocols. The ability to tailor their properties through deliberate modulation of composition provides avenues to tailoring geometric and coordination environments of SACs. Since its discovery in 2015 by Rost et al. [47], HEOs have continuously gained considerable attention as advanced functional catalyst systems with performances superior to conventional metal oxide systems. Design and application of SACs and HEOs catalysts have turned out to be very hot research areas in the field of advanced catalytic materials, therefore, stabilizing single atoms on HEOs has undoubtedly emerged as one of the most recent advances in catalyst design, combining the two emergent catalyst design approaches. Although several independent review papers have discussed SACs and the catalytic features of HEOs, far less attention has

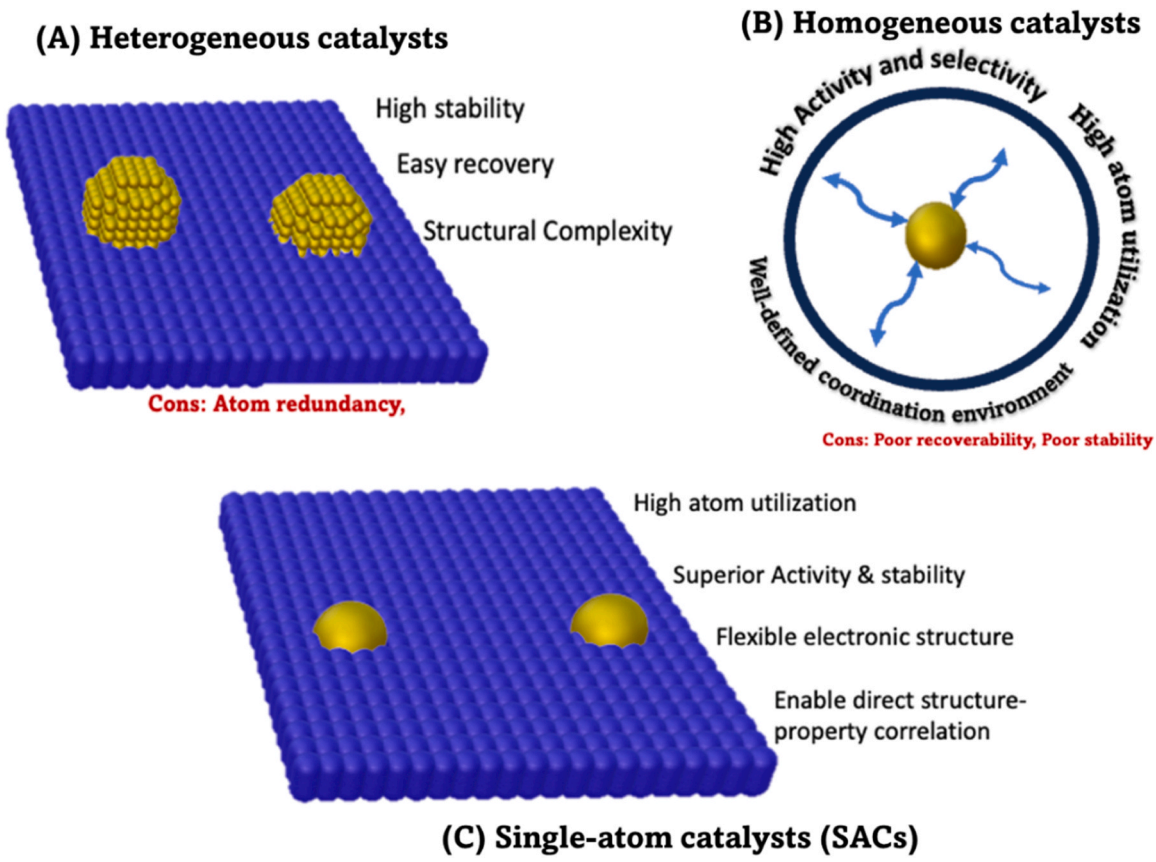

Fig. 1. A diagram shows a comparison of (A) heterogenous catalysts, (B) homogenous catalysts and (C) single atom catalysts (SACs) with their respective advantages and disadvantages.

been given to the possibilities that lie in HEO-supported SACs. With the growing interest toward utilizing HEOs as supports for SACs, a comprehensive review that emphasizes such novelty is timely.

This review article seeks to discuss recent advances in the application of HEOs as support materials for SACs and other catalyst systems. It is structured to highlight the following fundamental aspects. Firstly, we give an overview of HEOs, from discovery through thermodynamics and criteria for single-phase formation and emergent synthetic protocols well-suited for catalytic applications. Then, we discuss immobilization techniques for SACs and other catalyst dimensions on HEO substrates while focusing on loading capacity and stability under harsh conditions. This aspect is extremely important as differences in maximum loading capacities have been achieved from various methods. In the end, the catalytic performance and behaviours of reported HEO-supported SACs are elaborated and a prospective outlook for the field is highlighted.

2. High-entropy oxides (HEOs)

2.1. From multicomponent alloys to HEOs: a brief chronology

Over the years, tremendous efforts have been channelled toward developing structural complexities with tailored properties [48–50]. This has been demonstrated in the chronological advancement from traditional alloys and alloying techniques to more structurally complex and compositionally diverse structures. In 2004, research reported by Yeh et al. introduced the concept of high entropy alloys (HEAs) [48]. Almost simultaneously, Cantor et al. also demonstrated that it was possible to stabilize up to five different cations in equimolar or near equimolar quantities within a single-phase system which they referred to as 'multi-component alloy' without any reference to 'high entropy' [51]. Fundamentally, HEAs may be defined in terms of composition or configurational entropy [52,53] The composition-based definition assumes that HEAs are alloys derived from five or more principal elements, where each principal element may assume a concentration (c_i) from 5% to 35% while that (c_j) of the minor elements does not exceed 5% (Eqs. (1),(2)) [54]. This definition derives its roots from the early motivation to explore the compositional space of multicomponent alloy phases only, without any consideration of single phase stability or high entropy [51].

$$n_{major} \geq 5, 5\ at\% \leq c_i \leq 35\ at\% \quad (1)$$

$$n_{minor} \geq 0, c_j \leq 5\ at\%. \quad (2)$$

Conversely, HEAs may be defined in terms of the value of configurational entropy of the alloy. Contributions to the total entropy result from configurational (ΔS_{mix}^{conf}), vibrational (ΔS_{mix}^{vib}), electronic (ΔS_{mix}^{elec}), and magnetic dipole (ΔS_{mix}^{mag}) entropies. However, the contribution from configurational entropy is dominant during mixing. This definition distinctively classifies entropy stabilized alloys into low ($S_{conf} < 1R$)(where R is the universal gas constant), medium ($1.5R > S_{conf} \geq 1R$) and high entropy ($S_{conf} \geq 1.5R$) alloys [48,49,55]. Synergistic effects among the different metals and associated entropy driven behaviours within the crystal structure [56] provide HEAs with superior mechanical properties such as ductility [57], resistance to corrosion [58], and wear [59]. These unprecedented properties observed in HEAs as re-emphasized by several review articles [60,61] and have motivated further exploitation of the concept of entropy stabilization, which led to the discovery of a plethora of other entropy stabilized systems such as high entropy ceramics (HECs) [62,63], glasses [64], thermoelectrics [65], dichalcogenides [66], metal-organic-frameworks [67], polymers [68], sulphides [69], hydroxides [70] and recently exhibited in the assembly of high entropy Mxenes [71]. In 2015, Rost *et al.* reported the first entropy stabilized oxide system consisting of up to five different

cations in equiatomic ratios [47]. Analogous to HEAs, these entropy stabilized oxide systems were assigned the name HEOs [72,73]. However, as discovered by Rost et al. and further highlighted in several review papers, HEAs and HEOs are distinct in terms of cation arrangement and interactions within the crystal lattice [47,74]. While HEOs are often confused with entropy stabilized oxides (ESO), HEOs entail only having high configurational entropy, irrespective of the direction of enthalpy changes. However, true entropy stabilization entails having high configurational entropy that overcomes positive mixing enthalpy ($\Delta H > 0$). In this case, the high entropy is established as the driving force for phase stability at a specific temperature (T) [75] and the material exhibits entropy driven properties such as phase reversibility [47]. To stabilize a single-phase HEO system, the configurational entropy (S_{conf}) must be maximized to be greater in terms of TS_{conf} than the change in enthalpy of mixing (ΔH_{mix}) and consequently dominate the thermodynamic landscape of the reaction [76]. Such S_{conf} can be maximized by increasing the number of elements randomly distributed within the crystal structure [47,77]. The compositional diversity and the potential to modulate structural deformations in these compounds for optimal disorder provide infinite avenues to control and tailor its properties. These possibilities had obviously led to the development of HEOs with remarkable properties such as colossal dielectric constant [73], reversible energy storage [55,78,79], superionic conductivity at room temperature [78,79], photocatalytic [80,81], magnetic [82], etc. Evidence of the general interest in HEOs is the numerous review articles recently published [46,49,60,61,74] that attempts to uncover fundamental aspects such as advances in synthesis, compositional and structural diversities, state-of-the-art characterization techniques, applications, computational methods for structure and property probing, future prospects and possible problems to be addressed.

2.2. Thermodynamic criteria and descriptor-based models for single-phase formation in HEOs

Over the years, the Humme Rothery rules have been instrumental in predicting phases in a solid solution of binary alloys [83] as emphasized by various reports [84–86]. These rules basically rely on atomic size differences, and electronegativity differences between the participating atoms to predict favourable phases. They posit that if the atomic size difference between the components is greater than 15%, then the chances of forming a substituted solid solution become small. Also, a large electronegativity difference between the components or a more negative enthalpy of mixing favours a compound formation of not being solid solutions. Since these rules were formulated while considering simple two-component alloys, integration of up to five different atoms (in the case of multicomponent HEAs) with uniform probabilities of occupying the lattice sites, coupled with lattice distortions caused by a large atomic size difference of the components, induces fundamental structural deviations from the traditional alloys [84]. This suggests a fundamental limitation of the classical Humme Rothery rules in determining solid solution formation in HEAs. To evaluate the impact of atomic size difference (*Delta*) while considering such structural deviations from traditional alloys, Eq. (3) is used to estimate the Delta value [84].

$$Delta = \sqrt{\sum_{i=1}^{N} c_i \quad (1 - r_i \quad /\bar{r})^2} \tag{3}$$

where N denotes the number of components within a HEA system, C_i is the atomic percentage of the *ith* component, $\bar{r}\ (= \sum_{i=1}^{N} c_i r_i)$ is the average atomic radius, such that atomic radius is r_i [86]. Furthermore, electronegativity difference (Δx) is another important factor for assessing the suitability of solid solution in a multi-component system and can be calculated from Eq. (4) [84]. In principle, there should be some difference in the electronegativity of the cations [47].

$$\Delta x = \sqrt{\sum_{i=1}^{n} C_i (x_i - \bar{x})^2} \tag{4}$$

in which n represents the number of components within the alloy system, x_i is the Pauling electronegativity of the element *i* which can be found in [84], C_i is the atomic percentage of each element *i* in the alloy, while $\bar{x}$ represents the average electronegativity of the alloy system and can be evaluated from Eq. (5) [84].

$$\bar{x} = \sum_{i=1}^{n} C_i x_i \tag{5}$$

Mixing enthalpy ΔH_{mix} is another parameter used to evaluate the chemical compatibility of atoms in high entropy multicomponent atoms, expressed in KJ/mol. Also, as aforementioned, the high configurational entropy S_{conf} (> 1.5 R) in entropy stabilized multicomponent alloy systems plays a significant role in single phase formation of solid solutions at equimolar ratios [48].

Fig. 2 presents a summary of different HEO structures reported in the literature (A), and an HEO example using (MgNiCuZnCo)O to demonstrate entropy driven phase stabilization (B), the entropy distributions with increasing number of cations (C), the interplay between mixing entropy S_{mix}, atomic size difference (*Delta*) and mixing enthalpy ΔH_{mix}, and how such influences phase formation (D), and its phase evolution at different temperature. As shown in Fig. 2E, a single-phase is achieved only at temperatures exceeding 850 °C. As an entropy stabilized system, it shows reversible phase transformation with temperature cycling from 1000 °C (single-phase) to 750 °C (multi-phase) and back to 1000 °C (single-phase) [47].

Another important factor that affects solid solution formation in multicomponent systems is the valence electron concentration (VEC), which has been proven instrumental in determining the phase stability of intermetallic compounds, expressed as [85]:

$$VEC = \sum_{i=1}^{n} c_i (VEC)_i \tag{6}$$

where $(VEC)_i$ represents the valence electron concentration of the *ith* component and c_i is the atomic percentage of each element *i* in the alloy.

The studies in [84–86] have thoroughly examined the Hume-Rothery rules for solid solution formation and have identified the limitations and conclusively outlined various parameters which truly determine solid solution formation in multicomponent HEAs. Cumulative results from these studies as reported in [85] assert that high entropy alone is not sufficient to determine solid solution formation in multicomponent alloys in equiatomic ratios. For a solid solution to form in such a system, enthalpy of mixing, ΔH_{mix} (KJ/mol), atomic size difference (*Delta*) and mixing entropy (S_{mix}) must simultaneously satisfy; $-22 \leq \Delta H_{mix} \leq 7$kJ/mol), $0 \leq Delta \leq 8.5$, and $11 \leq \Delta S_{mix} \leq 19.5$J/(Kmol) [85]. At $Delta \geq 9$, the formation of bulk metallic glasses is favoured over solid solution formation. This makes atomic size difference a critical factor in designing a HEA solid solution. These constraints mean that, until such chemical and physical compatibility rules are obeyed, the formation of a solid solution is not favoured. All three conditions as stated by the Humme-Rothery rules agree with the popular Potential Energy Fluctuation model (PEF) [87]. Within the context of the PEF model, all three criteria as stated in the Hume Rothery rules can be summed up that low potential energy fluctuations favours solid solution formation [87,88].

Since this paper is primarily interested in HEOs and not the HEAs, discussion and data provided on HEAs will be limited. The information presented on HEAs is intended to serve as a reference starting point to the concept of entropy stabilization within a multicomponent system which extends to the HEOs system.

The feasibility of chemical reactions depends on the direction of free energy changes, and the Gibbs free energy change denoted by ΔG [60].

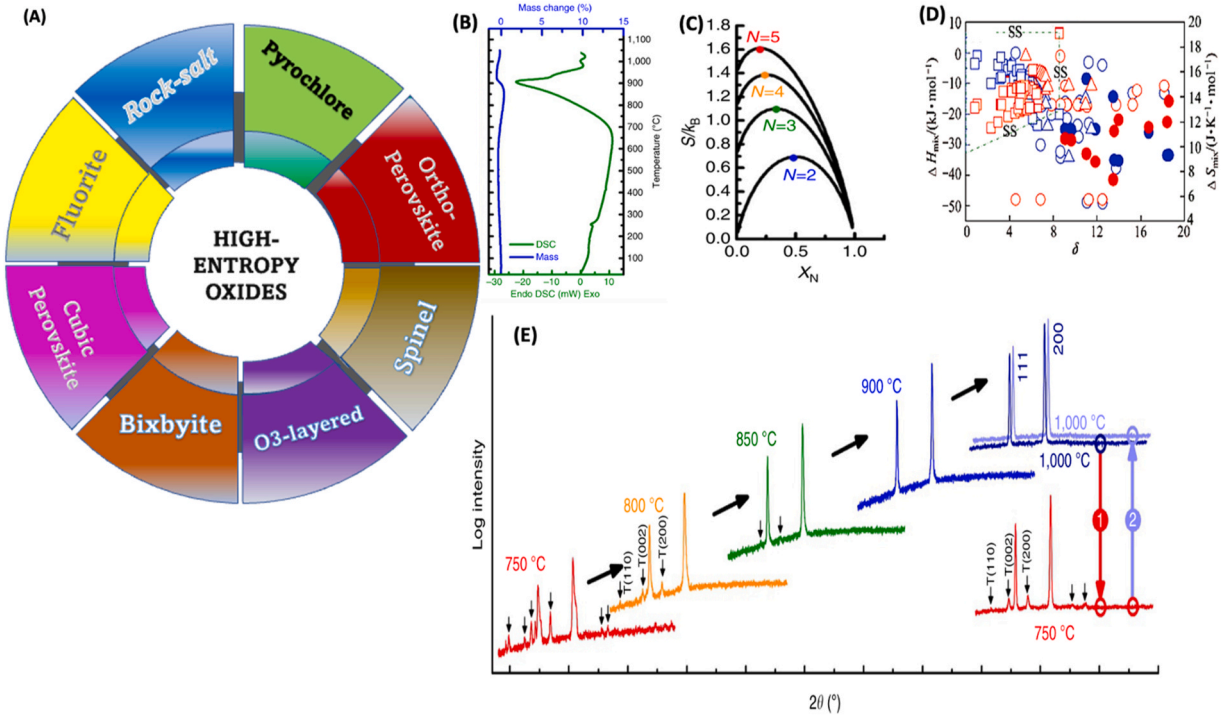

Fig. 2. (A) A summary of different HEO structures reported. (B) Differential scanning colometry conducted on high entropy (MgNiCuZnCo)O to demonstrate entropy driven phase stabilization [47]. (C) Calculated configurational entropy in an N-component solid solutions as a function of mol% of the Nth component where cations are present in equiatomic ratio [47]. (D) illustrates the interplay between mixing entropy S_{mix}, atomic size difference (*Delta*) and mixing enthalpy ΔH_{mix}, and how such influences phase formation [84,85]. The symbol ◦ represents equiatomic amorphous phase forming alloys; ● represents non-equiatomic amorphous phase forming alloys; □ represents solid solution phases and △ represents intermetallic phases. The region delineated by the dash-dotted lines indicates the requirements for solid solution phases. (E) Phase evolution of (MgNiCuZnCo)O with varying temperatures.

Within the context of HEOs, single phase stabilization is achieved only when mixing results in a reduction in Gibb's free energy ΔG_{mix} (j/mol) [89], given by Eq. (7) [52].

$$\Delta G_{mix} = \Delta H_{mix} \quad - T\Delta S_{mix} \tag{7}$$

where ΔH_{mix} represents the mixing enthalpy, ΔS_{mix} is mixing entropy and T is the temperature of the reaction. when ΔH_{mix} is extremely large, a high temperature is required to maximize the entropic term ($T\Delta S_{mix}$). Contrary to intuition, very negative ΔH_{mix} does not favour the formation of entropy stabilized single phase; instead, it favours the formation of intermetallic compounds. Generally, ΔH_{mix} close to zero favours the formation of single-phase entropy stabilized mixed metal oxides [76].

As defined by Sarkar et al., HEOs are single-phase oxide systems formed by combining up to five different cations such that the configurational entropy is greater than 1.5 R [49], Such high configurational entropy results from the random substitution of up to five cations in the same sublattice. As the configurational entropy associated with such mixing is key to achieving a single phase, it becomes important that its value be properly estimated. Several equations have been used to estimate the configurational entropy of various HEO structures. For example, for HEOs having the unit formula $A_xB_yO_z$ as in high entropy perovskite oxides (HEPOs), S_{conf} can be calculated using Eq. (8) [90].

$$S_{conf} = -R\left[x\left(\sum_{a=1}^{M} x_a \ln x_a\right) + y\left(\sum_{b=1}^{N} y_b \ln y_b\right) + z\left(\sum_{0=1}^{P} z_o \ln z_o\right)\right] \tag{8}$$

where x_a, y_b, and z_o represent mole fractions of elements located at the A-site, B-site, and O^{2-} site of the perovskite structure respectively. The M, N and P represent the number of elements at the A, B, and O^{2-} sites respectively. Contributions towards the configurational entropy are largely dominated by cations. If only oxygen is found at the O^{2-} site, then the contribution of the anions to total configurational entropy becomes negligible. The configurational entropy of HEOs having a single cation sublattice (e.g., Rocksalt or fluorite oxides) could be simplified as shown in Eq. (9) [90].

$$S_{conf} = -R\left[x\left(\sum_{a=1}^{M} x_a \ln x_a\right)_{cation\ Site}\right] \tag{9}$$

Unfortunately, estimations from these equations are based on ideal mixing assumptions, which is not the case in HEOs. Also, Eq. 6 suggests that the configurational entropy in HEOs is the same with HEAs having the same number of cations in equimolar ratios, however, this is not always the case as the total entropy associated with a single cation in HEOs is less than that in HEAs due to the regular arrangement of oxygen atoms in the oxygen sublattice. Fortunately, it provides reasonable approximations that have proven to be usable for HEO design. An effective way to predict solid solution formation in such mixed oxides from the perspective of thermodynamic rules of mixing is to consider the changes in chemical potential $\left(\frac{\partial G}{\partial n_i} = \mu_i\right)$ that accompanies the introduction of a new component *i*, to an already existing solid solution having *n* components [76]. To do this, McCormack et al. outline that the activity of component of $i(a_i)$ in solution, having both ideal and non-ideal contributions to mixing (see Eq. (10)) [76], is very important.

$$\Delta\mu_i = RT\ln\gamma_i + RT\ln X_i \tag{10}$$

where $RT\ln X_i$ is the partial molar entropy that results from the addition of components into the system (contributions to ideal mixing) while $RT\ln\gamma_i$ comprises the non-ideal component which is related to the partial enthalpy and partial excess entropy. This rule of mixing is particularly important in pushing the compositional domains of already synthesized single phase HEOs as it allows us to add components to an already existing single phase HEOs system.

Although the above thermodynamic rule of mixing has been sug-

gested for the addition of more components into an existing single-phase HEOs system, the criteria for single phase stability widely vary among different structures. For example, the initial construction of the divalent rock-salt $(NiMgCuZnCo)O_x$ HEO system by Rost et al. was guided by four major criteria: (i) there must be a difference in the crystal structure, electronegativity and cation coordination between the component binary oxides, (ii) the binary oxides are selected in pairs such that at least one pair does not exhibit excessive miscibility, for example, MgO-ZnO, CuO-NiO, and (iii) the entire collection should be isovalent [45]. Even though such rationale was not complete according to the most favourable conditions for solid solution formation under ideal mixing assumptions, it was adopted to clearly show the impact of configurational entropy on single-phase stabilization [47]. While this selection rationale is not in keeping with the classical Hume-Rothery selection rules as they included non-isostructural CuO (tenorite) and ZnO (Wurzite), such rationale was effective in forming the single-phase HEOs. From a thermodynamic point of view, structural transformations of $CuO^{tenorite \rightarrow rocksalt}$ and $ZnO^{wurzite \rightarrow rocksalt}$ induce a positive enthalpy penalty leading to a higher temperature for single-phase formation [76]. Unfortunately, selection rules based on isovalent cation combination only limit the choice of metals and consequently limit the compositional space of these materials. By carefully selecting element compositions that satisfy the geometric compatibility and electrical balance requirements in perovskites, Tang et al. successfully synthesized single phase high entropy perovskite oxides (HEPOs) with diverse elemental compositions having considerable size and valency differences [91]. Ideally, combining isostructural components having minimal size differences and valences is likely to favour solid solution formation. For perovskites, the Goldschmid structural tolerance factor (t) is given by Eq. (11) [92].

$$t = \frac{R_A + R_B}{\sqrt{2}\,(R_B + R_O)} \tag{11}$$

where R_A, R_B, and R_O represent the radii of A cation, B cation, and oxygen anion respectively [92]. To effectively carry out this study, substituted cations are first partitioned into different subsystems that ensure electrical stoichiometry. From those systems, another subsystem is formed by considering geometric compatibility. Generally, cations are selected such that their combinations are in accord with Pauling's first rule and Goldschimdt's tolerance factor. Based on these selection criteria, 12 subsystems were formed (cation valency is restricted to +2 to +6), 10 of which formed a single-phase cubic structure. Findings from their studies reveal that single-phase is formed when $0.97 \leq t \leq 1.03$; however, multi-phase is formed at $t \geq 1.03$. Conversely, the formation of partial ordering is controlled by cation valence mismatch $\delta(V_B)$ estimated from Eq. (12) [91].

$$\delta(V_B) = \sqrt{\sum_{i=1}^{5} C_i \left(1 - \frac{V_i}{\sum_{i=1}^{5} C_i \quad V_i}\right)^2} \tag{12}$$

where C_i and V_i represent the mole fraction and valence of the i^{th} cation. These results agree closely with previously reported results where phases produced are dependent on the values of t such that a cubic phase is obtained when $0.97 \leq t \leq 1$, a tetragonal of hexagonal phase when $t > 1.0$, and orthorhombic or rhombohedral phase is observed when $t < 0.9$ [94]. On the other hand, the electrical balance requires that the cation valence combination favours stoichiometry in the HEO formed [91].

HEPOs have recently emerged as a desirable system due to their unique properties and versatile areas of application. To that end, various attempts have been made to synthesize different HEPOs with different A-site, B-site, or both metal combinations. Predominantly, cations of similar valence in equimolar amounts have been used for the construction of these systems. Ma et al. [93] suggest that an opportunity for obtaining high performance HEPOs of the form $A(5B_{0.2})O_3$ exists by exploring aliovalent substitutions having non-equimolar amounts of cations. First, cations of appropriate valency are selected to achieve electrical balance followed by subsequent selection based on geometric compatibility in accord to Pauling's first rule and Goldschmid tolerance factors. Careful consideration of the vast data available on the construction of HEOs reveals that the criteria for achieving single phase synthesizability is rather unique for different structures [47,91,94]. Generally, HEOs design through aliovalent substitution of cations having different stable oxidation states, with ionic size differences exceeding the amount stipulated by the Humme Rothery rules, is yet to be fully explored.

Specifically, Usharani et al.'s work [95] on the synthesis of nanocrystalline $(CoCuMgNaNiZn)O_x$ (hereafter regarded as Na-TMO) in near equimolar ratios clearly demonstrates the possibility of stabilizing cations with different valency and cationic size, highlighting the unique role of aliovalency and non-stoichiometry. Herein, the sodium ions having an ionic size of ~ 47.8% relative to Ni^{2+} (which is the smallest ion in the system) were successfully incorporated into the rocksalt lattice of $(CoCuMgNiZn)O_x$ (hereafter regarded as ME-TMO) to form a stable single-phase HEO. Surprisingly, Ca^{2+} having the same stable oxidation state (+2) as the other cations and with a smaller ionic size difference (44.9% relative to Ni^{2+}) shows partial lattice solubility with the evolution of CaO secondary phases. This clearly demonstrates that the addition of cations with lower ionic size difference and valence mismatch will not automatically guarantee single phase formation. To further understand the most important parameters for single-phase formation in Na-TMO, X-ray photoelectron spectroscopy (XPS) was used to gain insight into the electronic structure and defects within the crystal lattice. XPS results reveal that the introduction of Na^+ induces some non-stoichiometry leading to an excess negative charge of 5.83. To compensate for this and regain charge neutrality, about 2.91% oxygen vacancies were created. However, 10.17% of the 50% cations assumed a lower oxidation state (Na^+ and Cu^+) which created a non-stoichiometric system that could not be fully compensated for by the creation of 2.91% oxygen vacancies. To fully ensure charge neutrality, cations such as Ni and Co assumed higher oxidation states and provided compensations of 0.80% and 3.55% respectively, indicating the significant role of Co in stabilizing the system. Furthermore, the addition of +3 oxidation state cations did not result in single phase HEOs. These studies suggest that multivalency is crucial in accommodating differences in ionic sizes toward single-phase stability [95].

A dependence of single-phase on elemental composition was studied by Djenadic et al. [96]. Rules of mixing like that for the divalent rocksalt were reported by Rost et al. [45], but slight modification was employed to synthesize several single-phase multicomponent rear earth oxides. Respective cations were selected such that at least one cation differs in crystal structure, coordination number, and valency, with minimal ionic size differences. However, XRD studies reveal that a single-phase CaF_2-type ($Fm\text{-}3m$) structure is only achieved with the inclusion of Ce^{4+} highlighting the unusual dependence on certain cation. Careful investigation of the rules employed to synthesize different HEO structures suggests that there is no one fix all rule for designing single-phase systems, but different rules should be explored to design different systems depending on the composition, structure, and interactions between the cations. For instance, combined experimental and computational studies by Li et al. [77] reveal that temperature, entropy, and oxidation environment (oxygen partial pressure) can be appropriately modulated to overcome the size difference constraints while achieving single phase multicomponent systems.

Based on above discussion, Fig. 3 summarizes major factors that control single-phase formation in HEOs. Firstly, the synthetic strategy adopted may interfere with the process to obtain single-phase HEOs (Fig. 3A). Specifically, Fig. 3B describes the perovskite oxide structure (ABO_3), clearly identifying the A and B site cations and an equation illustrating the limits of the tolerance factor (t) within which a stable perovskite structure is formed, thus guiding the selection of cations for the formation of single-phase HEPOs. Fig. 3C presents the factors

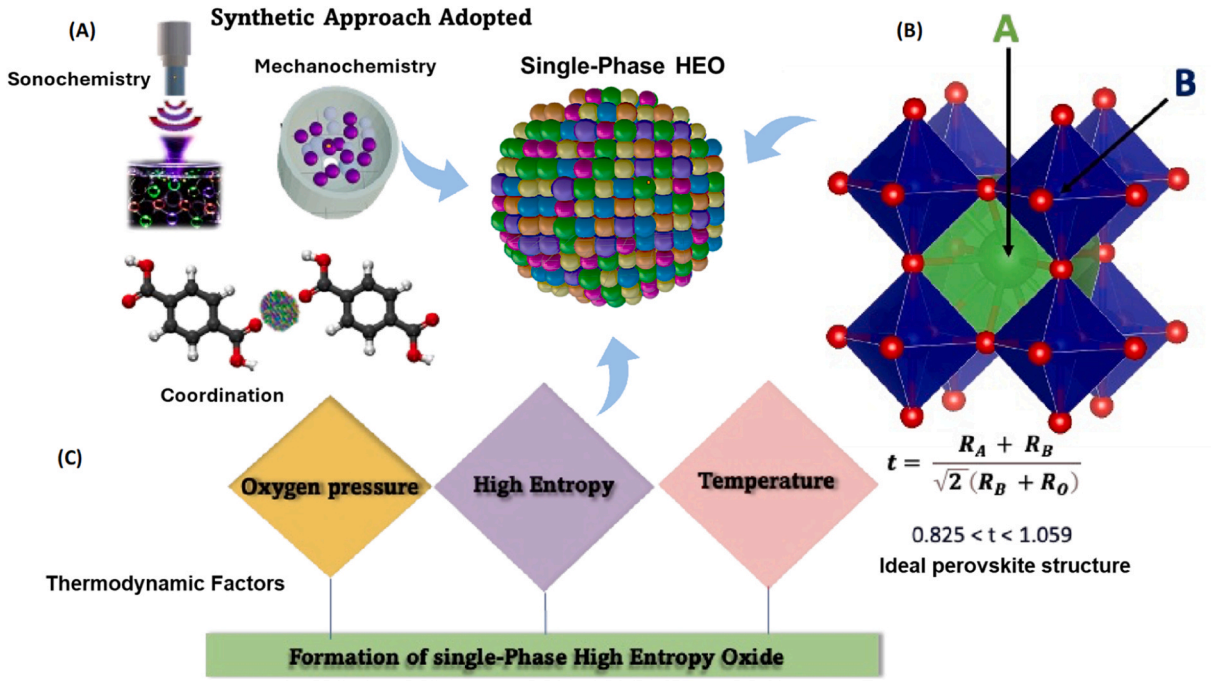

Fig. 3. Summary of controllable factors that affects single phase formation in HEOs. (A) Synthesis method adopted. (B) Goldsmith tolerance factor for perovskite oxide formation, which translates to high entropy perovskites. (C) Thermodynamic factors influencing single-phase formation in HEOs.

including geometrical compatibility and thermodynamic factors such as entropy, temperature, oxygen partial pressure to impact the single-phase formation of HEOs.

2.3. HEOs synthesis: emerging synthetic strategies for catalysis

Since the discovery of the first rock-salt entropy stabilized oxides (ESO) in [47], several HEO systems with diverse compositions and structures have been reported (see Fig. 2). The interest and success in this class of materials could be attributed to their unconventional properties as well as diversity in synthesis techniques. To date, a variety of synthetic methods spanning solid state techniques from ball-milling to wet-chemistry, such as nebulized spray pyrolysis, co-precipitation [95, 96], sonochemical [97,98], solvo/hydrothermal [99], solution combustion [100], molecular beam epitaxy and flame spray pyrolysis [101] and flame spray pyrolysis [102], have been successfully employed to synthesize HEOs. Regardless of the synthesis method adopted, the formation of a single phase in HEO systems relies on the entropic term ($T\Delta S$), which needs to be maximized above the enthalpy (ΔH) to dominate the thermodynamic landscape and compensate for enthalpic penalties associated with phase transformation [76]. Subsequently, most methods for HEOs synthesis mentioned above require thermal treatments under extreme conditions (900 °C-1200 °C) [47,91,93,95, 103]. Such high temperature treatments lead to uncontrollable crystal growth and pore collapse leading to HEOs with extremely low surface areas which are generally not desirable for catalytic applications [104].

2.3.1. Template-assisted synthesis of porous HEOs

Recently, novel synthesis techniques that either find a way to preserve pores during high temperature calcination (e.g., template-assisted synthesis) or totally circumvent the calcination process (such as sonochemical routes) have been reported. Template-assisted synthesis has over the years evolved as a very versatile method for synthesizing porous metal NPs. In this technique, templates such as mesoporous silica, mesoporous polystyrene, metal-organic framework, etc are used as hosts or molds for NPs. Subsequent removal of the template yields porous NPs. These techniques previously used for simple metal oxide NPs have been extended to synthesize porous HEOs. Figs. 4 & 5 present representative emerging template-assisted synthetic strategies for HEOs targeting at evolving structures with well-defined porous surfaces suitable for catalytic applications. Conventional methods of HEO synthesis occurring at elevated temperatures yield structures of low surface areas due to excessive particle growth under extreme thermal environments. To achieve surfaces with high porosity and site availabilities, several template-assisted methodologies ranging from mechanochemical to wet chemistry have been developed.

For example, Hou et al. [105] employed mechanochemical method using NaCl as a template to synthesize $Zr_{0.5}(NiFeCuMnCo)_{0.5}O_x$ with high surface area of 84 m^2g^{-1}. This strategy leveraged the ion-sharing ability of NaCl and its solubility in water. In this approach, a requisite amount of metal precursors and 2 g of NaCl were charged milling jar and milled for an hour. After that, a stoichiometric amount of NaOH was added to induce the formation of respective metal-hydroxides which is milled for an additional hour. The resulting HEO was recovered after sintering at 550 °C, washing off the NaCl in water, and vacuum drying at 70 °C (Fig. 4A). Fig. 4B presents synthesized porous $Pd/(CeZrHfTiLa)O_x$ featuring a high surface area of 162.1 m^2g^{-1} using template-assisted mechanochemical strategy [45]. To achieve the porous structure, an appropriate amount of metal precursors and fumed silica were milled followed by high temperature calcination at 900 °C to produce the corresponding HEO-SiO_2 template. The sacrificial silica was later etched out by washing with 2.5 M NaOH multiple times to obtain the corresponding porous structure.

Wang et al. [106] synthesized spherical mesoporous $(NiCoCrFeMn)O_x$ HEO with a single-phase spinel structure, featuring a surface area of up to 143 m^2g^{-1} and pore size up to 8.3 nm. To achieve this, wet chemistry sol-gel strategy was employed using a polyphenol as a polymerizable ligand to form a metal/polyphenol-formaldehyde metal--organic system. Calcination of the obtained metal-chelated spherical resin at 600 °C evolved the single-phase HEO (Fig. 5A). Single-phase $(FeNiCoCrCu)_3O_4$ with a surface area of 206 m^2g^{-1} was synthesized via a solvothermal method using metal-organic framework as a sacrificial template [99] (Fig. 5**B**). Similarly, as shown in Fig. 5C, mesoporous high entropy $(MgNiCuZnCo)O_x$ with holey lamellar structure

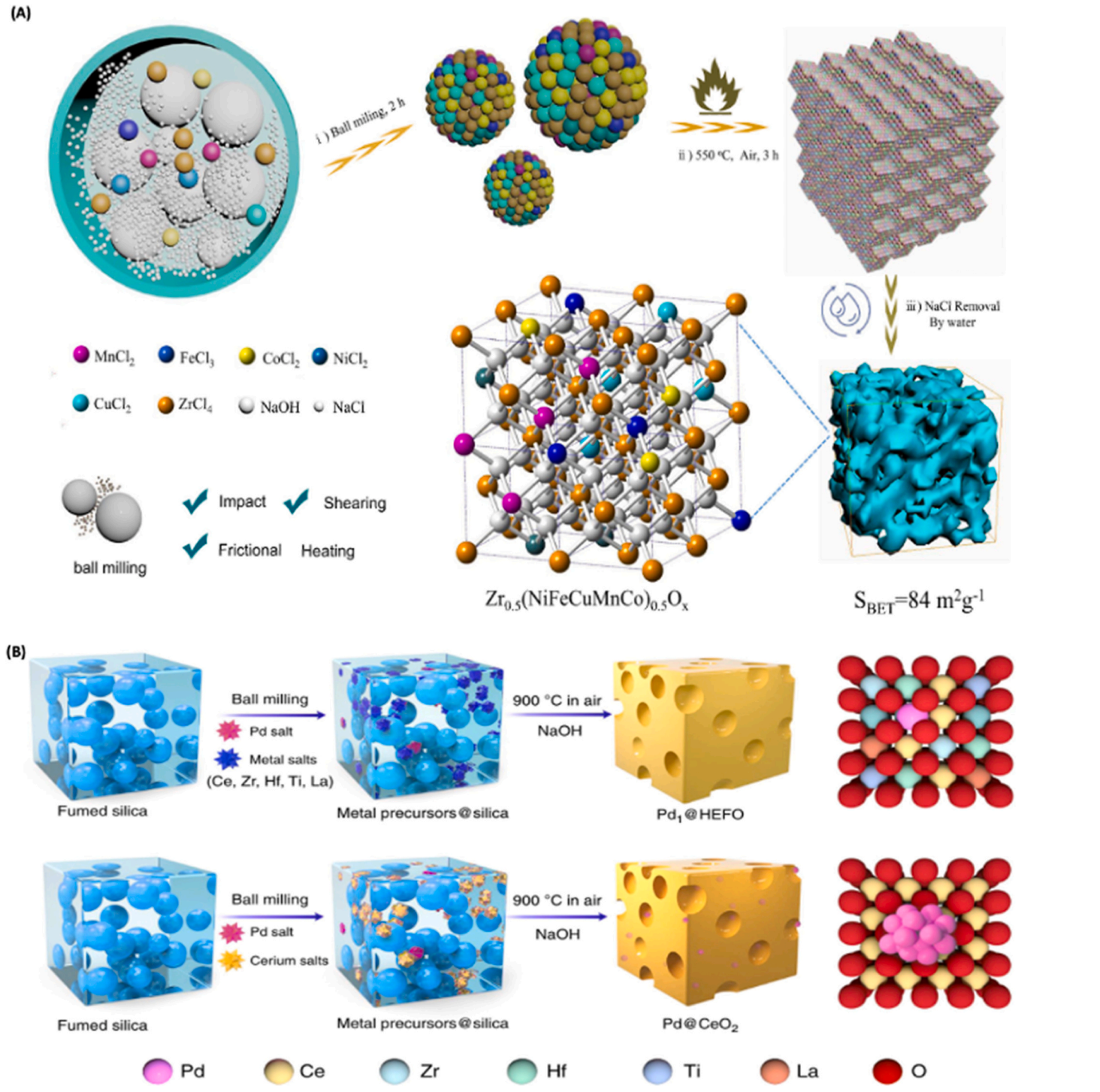

Fig. 4. Template Assisted strategies for synthesis of porous HEOs via mechanochemistry. (A) mechanochemical synthesis of porous $Zr_{0.5}(NiFeCuMnCo)_{0.5}O_x$ using NaCl as template [105]. (B) Template assisted synthesis of porous $Pd/(CeZrHfTiLa)O_x$ using fumed silica as sacrificial template [45].

synthesized via anchoring and merging GO as a template [107]. In Fig. 5D, a soft template-assisted strategy has also been adopted for synthesis of the mesoporous HEO thin films using block co-polymer Pluronic F-127 as a self-directing agent [108].

2.3.2. *Ultrasound-assisted synthesis of porous HEOs*

Pioneering work from Dai's group established the sonochemical technique as a facile method to synthesizing HEOs while circumventing the traditional annealing step [97,98]. This technique relies on cavitation energy released from high intensity ultrasound that produces local extreme environments, with temperatures exceeding 5000 °C and pressures above 2000 atmospheres in a times scale of 10^{-9} s. Essentially, the cavitation energy provides the necessary energy to induce crystallization and singe phase formation. Using this technique, they synthesized several HEPOs of the type ABO_3 with varying degrees of A and B-site substitution, with tremendous catalytic activity towards CO oxidation [97]. Similarly, they synthesized highly crystalline nanoporous high entropy $(CeHfZrSnEr)O_x$ with a cubic structure [98]. This technique holds great potential for low cost, easy, and facile synthesis of HEOs with good surface properties for catalytic applications [98]. To the

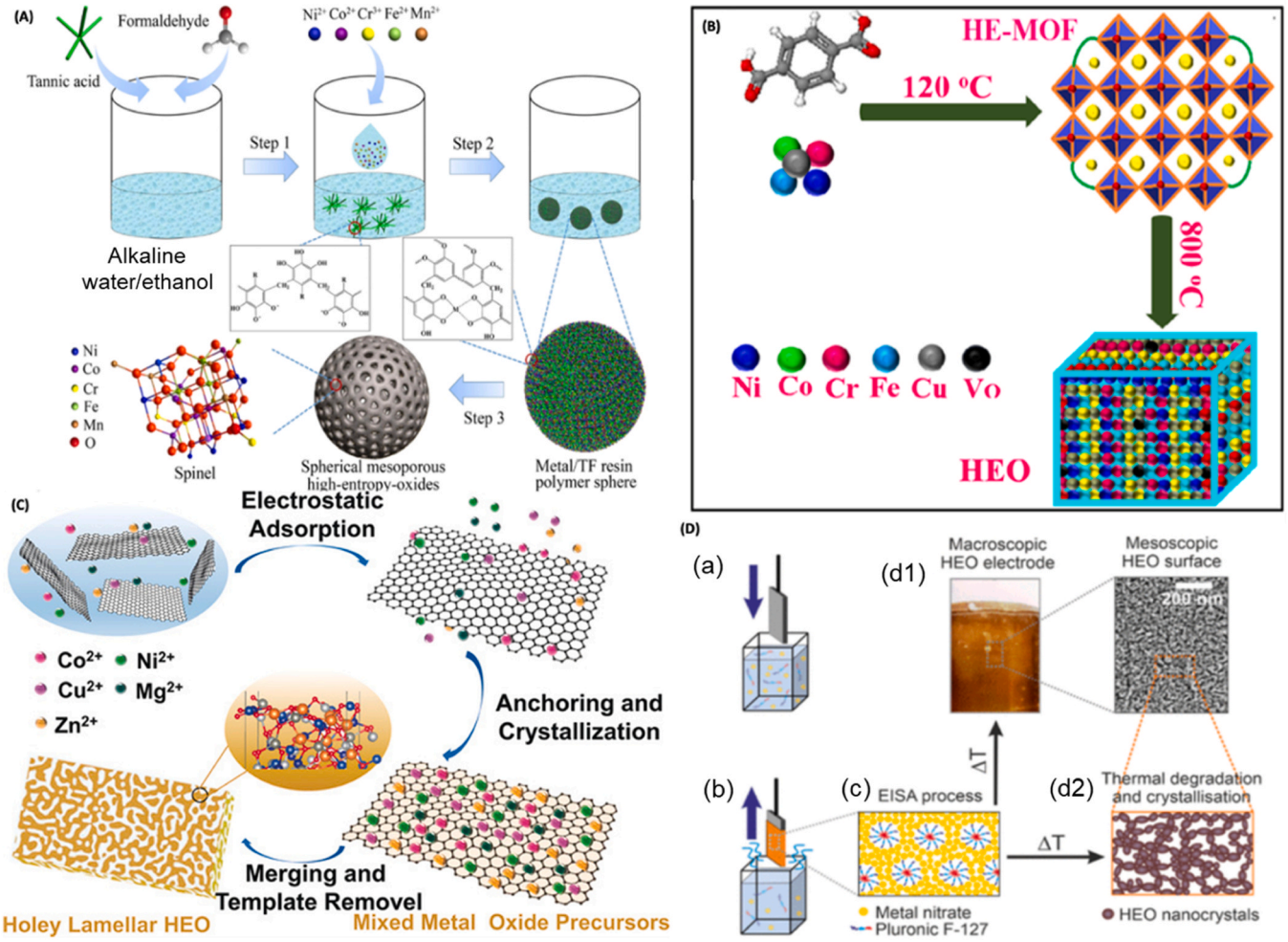

Fig. 5. Soft-templating strategy for HEO synthesis. (A) sol-gel route for synthesizing mesoporous $(NiFeCrCuCo)O_x$ [106]. Metal precursors are stabilized into a polyphenol-formaldehyde ligand to form a spherical metal-polyphenol-formaldehyde resin. Calcination at high 600 °C removes the organic ligand and the corresponding mesoporous HEO is obtained. (B) Porous high entropy $(NiCuCrFeCu)_3O_4$ obtained through solvo/hydrothermal route, using metal-organic formworks as sacrificial agent [99]. (C) Mesoporous high entropy (MgNiCuZnCo)O with holey lamellar structure synthesized via anchoring and merging using GO as template [107]. (D) Soft-template assisted strategy for synthesis of mesoporous HEO thin films using block co polymer Pluronic F-127 as self-directing agent [108].

best of our knowledge, only these two papers reported the synthesis of HEOs via sonochemical means, indicating a vast opportunity for research therein.

Fig. 6 represents the synthesis approach for HEOs via ultrasound treatment. This method becomes particularly beneficial as it circumvents both the need for templates and thermal treatments altogether and produce materials with optimal surface areas within a short reaction time. Fig. 6A shows a typical synthesis protocol during ultrasound synthesis of HEOs. Using such technique, single phase $(CeHfZrSnEr)O_x$ was successfully synthesized [98]. The single-phase cubic structure along with its microstructural properties are shown in Fig. 6B-C. This method is highly desirable as it evolves single-phase HEOs with adequate surface porosity in a very short time.

2.4. Computational methods for HEO design and property studies

Density Functional Theory (DFT) has emerged as a powerful tool for investigating the properties of materials of varying complexities, ranging from single atoms to high entropy oxides [109,110]. DFT calculations afford the direct prediction of a range of material properties such as thermodynamic stabilities, electronic structures, defect formation energies etc. with appreciable degrees of accuracy [111]. With such capabilities, DFT permits the facile screening of a large configuration space, enabling the discovery of a new materials with desired properties. Within the scope of HEOs, DFT is employed for a range of predictions ranging from phase stability, electronic structure, defect formation and reaction free energies at active sites. Utilizing DFT is particularly beneficial for systems like HEOs due to their vast compositional space and structural diversity, making predictions based on intuition or trial and error non-sustainable and inefficient. Several studies have reported the use DFT to make important predictions about the parameters related to thermodynamics of phase stability or catalytic properties of synthesized HEOs.

2.4.1. Density functional theory (DFT) and beyond for structural and electronic elucidation

Drawing foundations from thermodynamic rules of mixing where the type and number of components within a system of HEOs significantly affect solid solution formation under non-ideal scenarios [47,75,76,108] Anand et al. [112] applied classical potential simulation to investigate the impact of decreasing the number of components and also varying the type of component in (NiMgCoCuZn)O on the configurational entropy and enthalpy, which shows a direct bearing on phase stability. Such simulation was conducted using a GULP-code geometrically optimized rocksalt lattice, consisting of 1000 cations and 1000 anions. In their studies, they employed random, systematic, ordered, swapping as well as genetic algorithm sampling strategies to generate the various configurations. Findings from their studies revealed that phase stability is

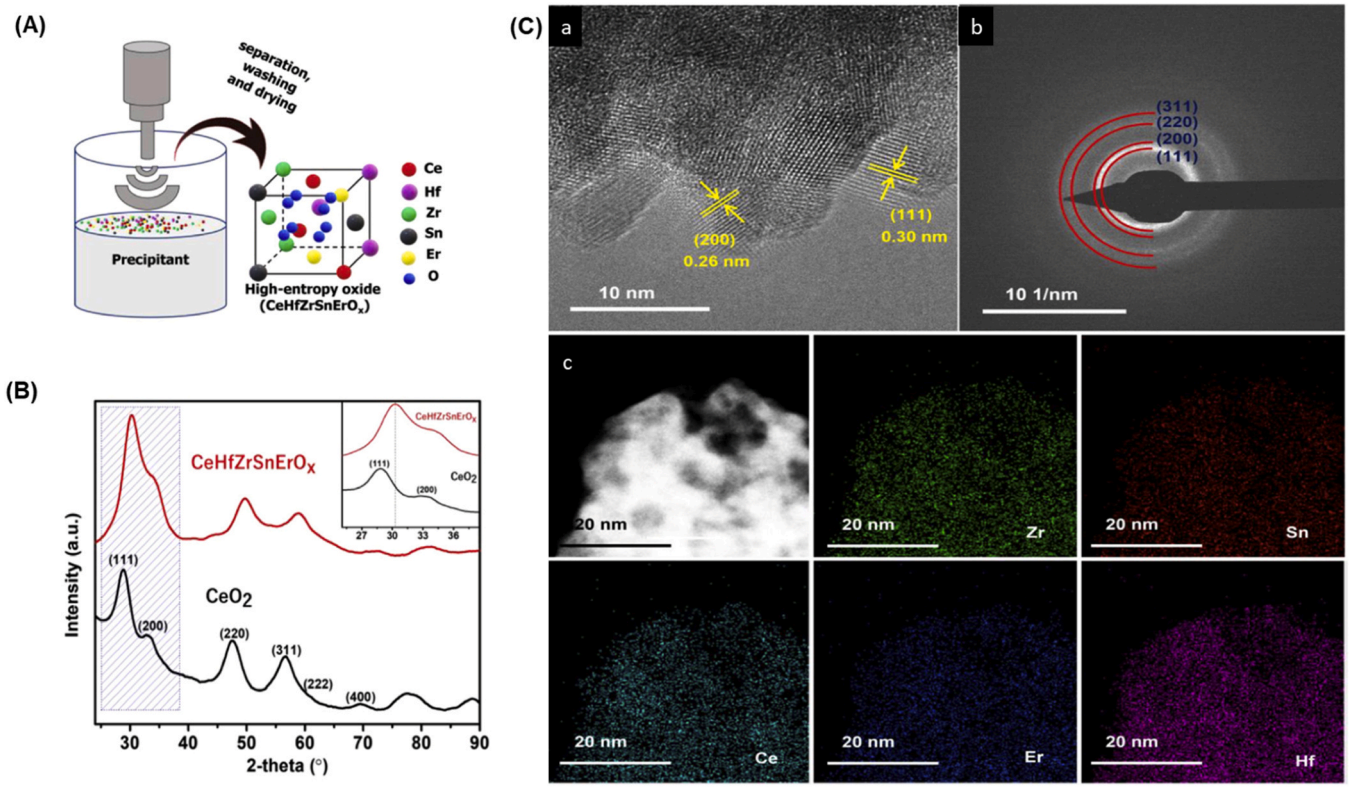

Fig. 6. A ultrasound synthesis method for HEOs. (A) Sonochemical approach for synthesis of high entropy (CeHfZrSnEr)O_x. (B) XRD pattern showing formation single phase (CeHfZrSnEr)O_x, exhibiting similar diffraction pattern with single-phase cubic CeO_2. (C) HR-TEM image of synthesized (CeHfZrSnEr)O_x, showing highly crystallized structure with well-defined lattice fringes corresponding to (200) and (111) planes of the cubic structure (a), SAED pattern of (CeHfZrSnEr)O_x with diffuse rings indicating polycrystallinity (b), and HAADF with EDS elemental maps showing well dispersed cations within the (CeHfZrSnEr)O_x system (c) [98].

achieved with high configurational entropy which is maximized by increasing the number of components. Also, the enthalpic penalty associated with phase transformations of ZnO and CuO leads to a higher temperature at which free energy is minimized to zero. Bond distance analysis reveals Jahn Teller type distortions around Cu^{2+}. As expected, the enthalpic penalty associated with the addition of cations reduces as the configurational entropy rises [76]. Entropy stabilization is achieved at temperatures where the free energy is minimized to zero. A similar study using DFT predictions combined with experimentation to explore compositional changes in formation energies and the resultant crystalline structure of HEO was reported [113]. Its DFT predictions showed results to agree with experimental results.

Fig. 7 shows some key findings pertinent to HEO design and properties that are derived through computational approaches. Fig. 7(A-B) presents mixing enthalpy because of the number of cations and composition, and also temperatures at which change in Gibbs free energy for each combination becomes zero. These results demonstrate the power of computational tools in probing the nature of these classes of materials.

Since cations are carefully selected to ensure charge neutrality within the HEOs [91], Rak et al. [114] conducted a DFT study to probe the possible impact of electroneutrality and electronic state changes as a function of composition on the structure and properties of HEOs and to check if an expression for predicting phase stability could be constructed from such relationships. In their studies, three HEO systems were used: $(Mg_{0.1}Co_{0.1}Cu_{0.1}Ni_{0.1}Zn_{0.1})O_{0.5}$ (termed J14), J14 + Li, J14 + Sc, and the DFT simulation was executed using the Projector Augmented wave (PAW) method. Such predictions suggest that the average lattice constant of the ternary structures provided good approximations to that of random structures. Also, such studies reveal that in J14, the Bader charges are transferable between the binary, ternary and random structures, while those of J14 + Li and J14 + Sc could be estimated from the average values of ternary compositions only. The findings create an avenue to develop an expression for ionic bonding in such a disordered structure. After numerous DFT probing into electronic state transformations that accompany each modification of the J14 system, the authors claim that empirical stability parameters for HEOs might be more complicated than those of HEA. Also, similar to results reported by Usharani et al. [95] where introduction of the monovalent Na^+ having larger ionic radius was accompanied by the oxidation of cobalt and nickel to Co^{3+} and Ni^{3+}, the DFT studies suggest that incorporation of the differently sized Sc^{3+} and Li^+ into J14 is accompanied by the reduction of Cu and oxidation of Ni, Cu, and Co. As expected, average distortion of individual elements from the ideal rocksalt lattice sites was higher in J14+Sc than in J14+Li. This was attributed to the fact that the addition of Sc enhances the reduction of Cu atoms as 8 out of 40 Cu atoms in the J14+Sc system show displacement of more than 0.5 Å **(**Fig. 7**C),** a highly disordered local M-site structure. However, distortion of the TiO_2 octahedron and chemical short-range ordering of Ti is observed in $Nd_2(Ta_{0.2}Sc_{0.2}Sn_{0.2}Hf_{0.2}Zr_{0.2})_2O_7$. Their calculations indicate that such ordering is energetically favoured and not due to sample processing.

Additionally, Rak et al. [116] confirmed Jahn-Teller type distortions associated with Cu^{2+} within the CuO_6 polyhedra. Such structural and electronic assessment was carried out within DFT using the plane waver PAW pseudopotential method. Calculated Cu-O bond length and density of states analysis indicate that approximately 10% of the Cu^{2+} undergoes such distortion. Such structural compression was ascribed to fundamental lattice constrains where competition exists between the elongated configuration preferred by Cu^{2+} centres and the normal octahedral configuration preferred by other cations. Their studies provided significant insights into the electronic structure and

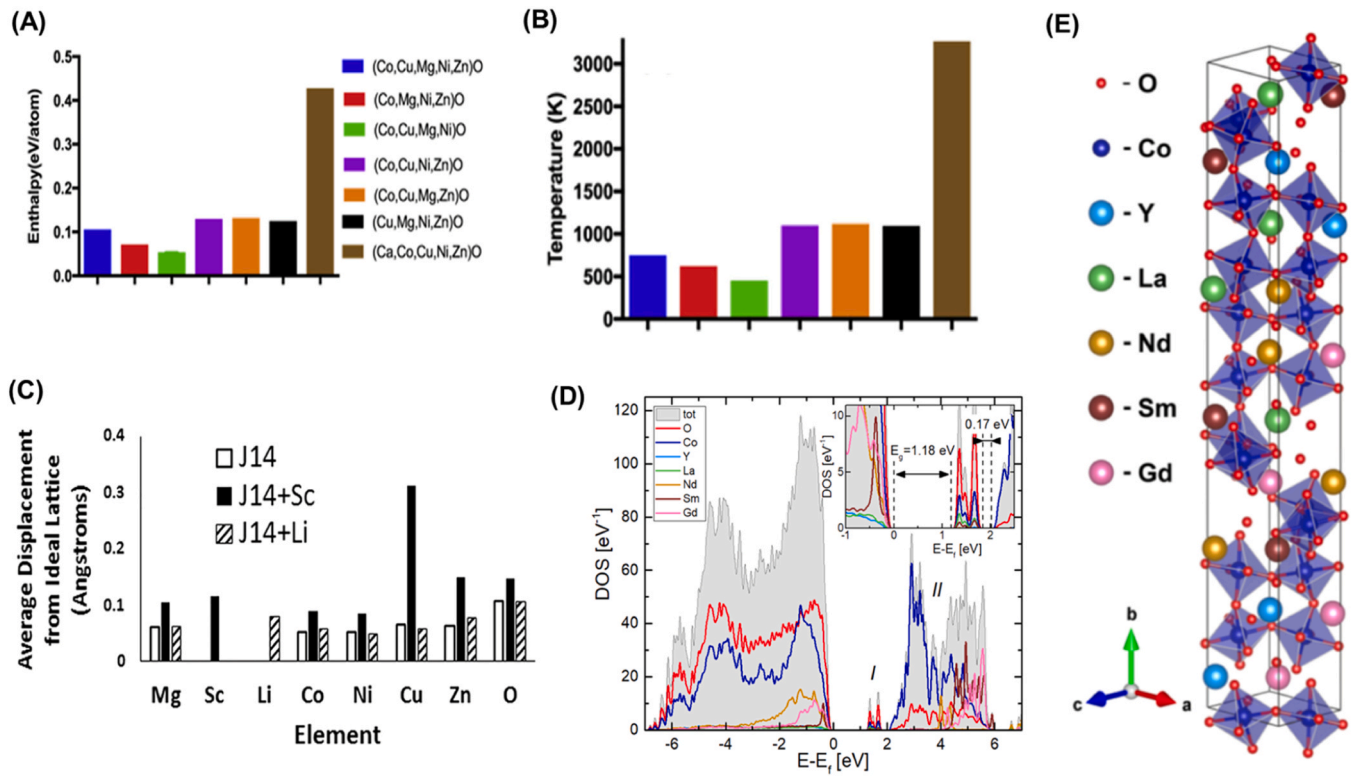

Fig. 7. (A) Variation in enthalpy of mixing for different oxide systems. (B) Temperature at which Gibbs free energy of mixing becomes zero [112]. (C) Average displacement from the ideal rock salt lattice sites for the three large random systems as a function of element type [114]. (D) Electronic structure of single phase orthorhombic ($Gd_{0.2}Nd_{0.2}La_{0.2}Sm_{0.2}Y_{0.2}$)$CoCO_3$) modelled using DFT implemented in Vianna ab initio simulation Package (VASP) while adopting a *Pnma* symmetry (1 ×5×1), a cell which contains 20 cobalt atoms and 60 oxygen atoms was constructed. Density of state analysis reveals that material is semi conducting with an estimated band gap of 1.18 eV [115]. (E) is the relaxed elementary cell used in DOS calculations [115].

crystallographic environments of the Cu^{2+} within entropy stabilized oxides. Another study by Rost et al. [117] conducted a complementary X-ray absorption fine structure (XAFS) and DFT to investigate the local environment of the cations and to examine how the disorder within the cation polyhedron is accommodated by the oxygen sublattice while focusing on the Jahn-Teller distortions around Cu. Generally, data from XAFS and DFT agree with the fact that oxygen is displaced from their original configurations to accommodate such disorder arising from cation-oxygen bond length.

2.4.2. *Density functional theory (DFT) for catalytic studies*

The compositional diversity of HEOs makes it challenging to predict active sites and reaction mechanisms for catalytic reactions. The different local atomic environment within HEOs leads to a distribution of binding energies for catalytic intermediates. Svane and Rossmeisl [110] recently deployed DFT for the practical determination of binding energies at different active sites on the (110) plane of high entropy $Ru_{0.2}Ti_{0.2}Ir_{0.2}Os_{0.2}Rh_{0.2}O_2$, using the oxygen evolution reaction (OER) at model reaction. To achieve that, they considered two possible pathways by which intermediates interacts with the active sites: via the coordinatively unsaturated sites and via proton transfer to bridging oxygens. They found out that the optimal performance varied with the reaction pathway considered. While considering adsorbate-surface interaction via the coordinatively unsaturated sites, large Ti amounts gave optimal performances however, in the bridge pathway, a mixture of Ru, Ir and a smaller amount of Rh was optimal. This study provides a more conclusive framework for probing and reporting the most favourable active sites within HEOs. Similarly Katzbaer et al. [118] deployed DFT to describe the origins of band gap narrowing observed in high entropy $(Fe_{0.2}Co_{0.2}Ni_{0.2}Cu_{0.2}Zn_{0.2})Al_2O_4$. Such narrowing observed in the HEO relative to the parent spinel arise from broadening of the energy distribution of the 3d states caused by differences in electronegativities and crystal field splitting across the 3d transition metal series. Such electronic structure changes within the HEO have been shown to directly enhance its OER performance relative to the low entropy parent spinel. This approach provides another way to probe synergistic interactions within HEOs towards making structure-property correlations. In another study, Gu et al. deployed DFT to precisely point out metal centers at which the OER process favorably occurs within an oxygen-vacancy engineered HEO surface [103]. Similarly, Nguyen et al. adopted both experimental and DFT approaches to benchmark various La-based high entropy perovskite oxides (HEPOs) for the OER process [44]. Among other HEPOs La(NiMn2CoCrFe)O_x showed highest intrinsic performance due to higher Co^{3+}/Co^{2+} ratios. DFT calculations, reveals that the OER process on HEPOs surface occurs via the adsorbate evolution mechanism (AEM) with formation on M-*OOH as the rate determining step.

However, utilizing DFT for predicting the properties of HEOs may suffer some fundamental limitations such as inability of some standard exchange-correlation functionals frequently used in DFT to accurately capture the intricate electronic interactions between elements in HEOs. Also, the computational cost of DFT calculations is prohibitively expensive, especially when studying HEOs having relatively large unit cells with dynamic compositions [111]. This computational demand may limit the exploration of extensive compositional spaces and hinder the comprehensive development of high entropy oxides. Fig. 8 summarizes the DFT approach as tools used for studying different aspects of HEOs.

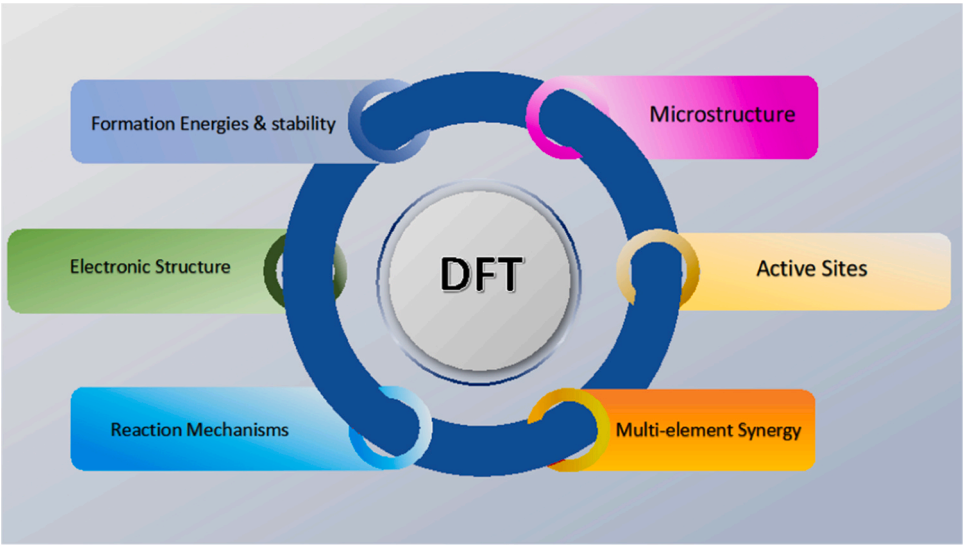

Fig. 8. General properties probed in HEOs using DFT.

3. Single-atom catalyst (SACs): origins of superior catalytic performance

3.1. SACs on metal-oxide supports: nature of bonding and electronic interactions

As established in earlier sections of this article, the SACs constitute atomically active metal centres which are stabilized on a support material [119]. Such atomic dispersion of metal active centres significantly boosts the atom utilization of the catalysts (higher ratio of participating atoms). As a result, SACs have in general demonstrated superior catalytic activity, selectivity, and stability when compared to their bulk counterparts [120]. Such improved properties have been associated with their highly flexible electronic environment, undercoordination [121] and metal-support interactions [34,38,122]. Understanding how all these factors directly regulates the catalytic performance of SACs are highly beneficial towards rational design of SACs with optimal performances. To illustrate this approach, we focused on SACs stabilized on metal oxides, with key emphasis on the nature of metal-support interaction, coordination environment and electronic structures.

Metal oxides have emerged as desirable supports for SACs for several important reasons such as their intrinsic stability under harsh chemical or thermal conditions, surface reducibility and abundant sites for SACs stabilization. Fundamentally, SACs may be anchored on the edges, corners, steps, vacancies, and surface OH groups available on the metal oxide supports. For the sake of understanding, we explain the bonding nature and chemical reactivities of SACs by delving into the unique chemistries of different SACs stabilized on FeOx, and CeO_2 supports as follows.

3.1.1. SACs supported on FeO_x

The first SAC reported features single Pt atoms stabilized on reducible Fe_2O_3 surface (Pt_1/FeO_x). The experimental characterizations corroborated with thorough density functional theory (DFT) calculations reveal that the Pt atoms preferred the three-fold hollow sites on the O_3-terminated surface of Fe_2O_3(001) [33]. DFT calculations reveals that Pt atoms favourably coordinated to three surface O atoms and a subsurface Fe, indicative of the substitution of surface Fe with Pt. Such substitution lowered the oxygen vacancy formation energies on the Fe_3O_4 (001). Bader charge analysis shows that the Pt sites were positively charged (+0.45), suggestive of an electron transfer from Pt to the Fe_2O_3 support. The CO adsorption strength follows the order Fe_2O_3> Pt_{10}> Pt_1/Fe_2O_3. The high activity of Pt_1/Fe_2O_3 towards CO oxidation was accrued to a reduced d-orbital charge density which modulates the binding strength of CO to the active sites. Similarly, Du et al. stabilized single Pd atoms on Fe_2O_3 (Pd_1/Fe_2O_3) via co-precipitation, with a Pd loading of 0.05 wt%. Extended X-ray adsorption fine structure (EXAFS) reveals Pd-O coordination without any Pd-Pd bond, indicative of isolated Pd single atoms instead of Pd NPs [120]. Such Pd-O bond is associated with single Pd atoms chemically coordinated surface oxygen of the support. Strong metal support interaction between single Pd atoms stabilized on the Fe_2O_3 initiates the dynamic carburization of Fe_2O_3 to form a highly active Fe_5C_2 layer, leading to enhanced reverse water-gas shift reaction. On the contrary, Pd NPs stabilized on the same support significantly inhibited the carburization process over time. Also, Pd stabilization significantly lowers the lattice oxygen activation energy. This suggests the unusual nature of metal-support interaction in SACs when compared to their NP counterparts. Previous reports have also confirmed the stabilization of single metals atoms of Pd, Pt, within the subsurface Fe vacancies of Fe_3O_4 (001) [123,124]. Such strong anchoring within the Fe vacancies is enabled by charge and orbital ordering within the subsurface layer [125]. Chen et al. uncovered the size effects of Pt single atoms and Pt NPs towards the water gas shift reaction (WGS) [126]. From their study, the size effect entirely changes the reaction mechanism, with the Pt single atoms having optimal specific reaction rate and turn over frequencies. For the SAC Pt_1/FeO_x, water molecules are first activated by oxygen vacances on the FeO_x surface to yield H_2 and O. The CO molecules moderately bonded to the Pt easily react with the O atoms to produce CO_2. On the contrary, the reaction follows a rather different pathway on Pt NPs stabilized on FeO_x. The H_2O molecules are activated to release OH. Also, the CO is strongly bonded to the FeO_x therefore reacts with the OH to produce intermediate, which then decomposes to form CO_2 and H_2. Fig. 9 depicts the features of SACs stabilized on FeO_x type supports in water gas shift reaction and a comparison to Pt NPs. The unique geometric and electronic nature of SACs alters key components of a chemical reaction such as changes in reaction mechanism, lowering of oxygen vacancy formation energies and synergistic interaction with the supports for form active sites.

3.1.2. SACs supported on CeO_2

The CeO_2 plays an important role in catalysing thermochemical reactions by acting as supports for a variety of highly active metals such as Pt, Au, Pd [127–129]. The unique Ce^{4+}/Ce^{3+} redox property, high defect formation tendency and reversible oxygen vacancy formation of CeO_2 render it very attractive as support for SACs [130–132]. Although

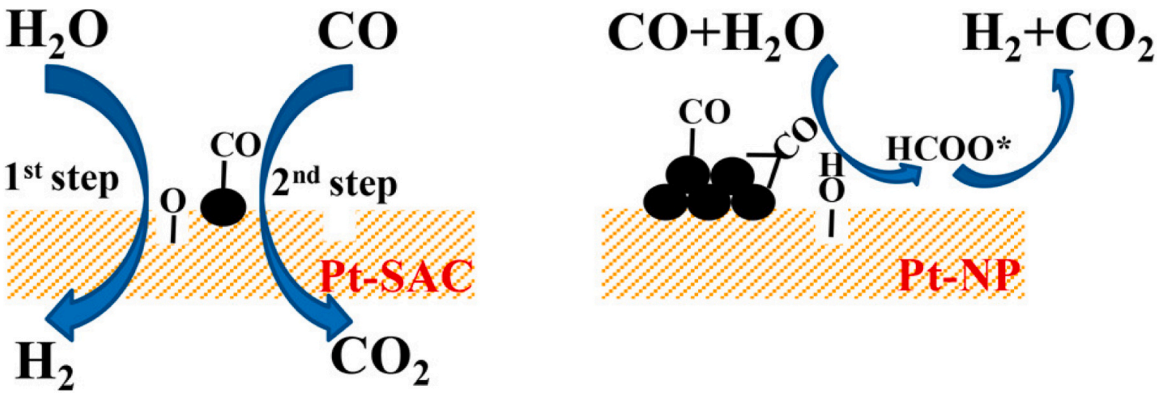

Fig. 9. (A) different reaction pathways for Pt single atoms (Pt-SAC) and a Pt-NP stabilized on FeO_x towards water gas shift reaction (WGS) [126].

CeO_2 supported catalysts are widely deployed for several important industrial reactions, there is still debate about the actual active sites during reactions. Lei et al. stabilized Au single atoms, clusters, and NPs on CeO_2 and explored their performances towards alcohol oxidation [128]. Experimental results and DFT studies reveal that oxygen vacancies (O_v) formed at the O-O_v-Ce-O-Au sites adsorb the alcohol molecules with subsequent O-H activation, while the adjacent Au^{3+}/Au^{2+} catalysed the elimination of ß-hydride in the alkoxide intermediate. However, single Au atoms have shown to promote the formation of O-O_v-Ce-O-Au sites compared to its cluster or NP counterparts. This resulted in higher catalytic responses for the SAC Au_1/CeO_2. Although this result did not solve the active site dilemma, it provides a fundamental way of tracking activity descriptors when comparing SACs with NPs.

Lee et al. [133] reported that Pt single atoms stabilize on CeO_2 surface by anchoring to surface oxygen to form Pt-O-Ce. Formation of such bond is highly promoted under oxidative conditions and at higher temperature. However, exposure to reducing environments during reactions triggers the elimination of surface oxygen and subsequent formation of oxygen vacancies (O_v) on the CeO_2. This leads to anchoring of the Pt atoms within O_v and elimination of the Pt-O-Ce bond. Such surface reconstructions drastically lower the thermal stability of Pt/CeO_2, revealing the cause of SAC aggregation under thermochemical conditions. Fig. 10 below illustrates the dynamic nature of SAC-support interface under different chemical environments.

Similarly, Muravev et al. probed the stability of Pd/CeO_2 prepared by flame spray pyrolysis (FSP) and the Pd/CeO_2 prepared by the impregnation of Pd unto hydrothermally synthesized CeO_2 nanorods [134]. Pd/CeO_2 via FSP showed higher catalytic performance towards low temperature CO oxidation. Such difference is underpinned by divergent nature of Pd-CeO_2 interface under testing conditions for both catalysts. Pd stabilized on CeO_2 nanorods shows high surface reducibility that leads to Pd agglomeration. Meanwhile, the Pd^{2+} in Pd/CeO_2 (FSP) is preserved under similar conditions. Such enhanced stability has been linked to higher surface lattice oxygen mobility in Pd-doped FSP catalysts. This reveals the immense contribution of synthesis method adopted in redefining the interfacial chemistry of SACs stabilized on CeO_2 supports.

4. SACs stabilized on HEOs: fundamental aspects and catalytic performance

In addition to the direct utilization of HEOs as catalytic active sites for various catalytic transformations, HEOs have been used as robust supports for single atoms, clusters, and NPs. The later usage of HEOs is motivated by their intrinsic ease for defect formation caused by the substitution of differently sized cations within the same lattice [95], the presence of oxygen vacancies [103], and high chemical and thermal stabilities [45]. The high chemical and thermal stabilities are particularly important to ensuring the formation of metal-support bonds that are strong enough to withstand sintering or agglomeration under harsh chemical or thermal environments [41]. Such high temperature stabilities demonstrated by HEOs surpass that of conventional metal-oxides. For example, high entropy $Zr_{0.5}(NiMnFeCuCo)_{0.5}$ exhibits entropy driven exsolution–dissolution phenomena to prevent sintering of active sites under harsh reducing environments [105]. Such intrinsic stability has found tremendous usability especially in synthesizing noble metal SACs for catalytic reactions occurring under harsh chemical or thermal environments. This informs the reason why majority of HEO supported SACs reported so far have been applied for thermocatalytic reactions occurring under elevated temperatures and pressure over an extended period.

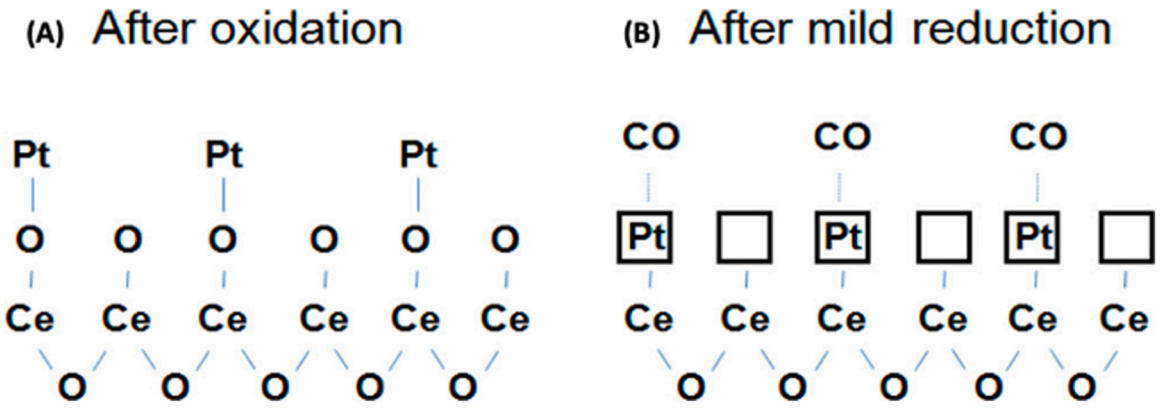

Fig. 10. (A) Pt anchored on CeO_2 surface via Pt-O-Ce after oxidative treatment. CeO_2 surface is oxidized. (B) after reductive treatment, CeO_2 is reduced and accompanied by formation of oxygen vacancy. Pt atoms are anchored within such oxygen vacancies [133].

To synthesize SACs, several techniques which could be classified as wet chemistry, physical and chemical deposition, photochemical, high temperature pyrolysis, galvanic replacement, and the more recent mechanochemical strategies have been explored to stabilize single atoms on various substrates [1]. To date, only a few of these methods have been successfully employed to stabilize SACs on HEOs. This is because some of these processes do not meet the basic conditions such as very high synthesis temperatures necessary to form the single-phase HEO support. While it is possible to synthesize metal oxide supports with subsequent stabilization of the single atoms in two individual steps [40], most SACs stabilized on HEOs are simultaneously synthesized, leading to the distribution of the single atoms not only on the surface but throughout the bulk of the HEO supports, making them entropy stabilized [45,104,135,136].

4.1. Characterization techniques for SACs supported on HEOs: an overview

To successfully characterize SACs supported on HEOs, careful characterization of the HEOs as well as the stabilized single atoms is essential. The initiative is primarily concerned with confirming the formation of HEOs as well as ensuring the homogenous distribution of single atoms within HEO systems. Information regarding (i) the formation of corresponding single-phase HEO, (ii) the homogenous distribution of constituent cations (iii) the molar ratios of constituent cations for configurational entropy estimation, and (IV) the electronic or chemical state of the atoms should be studied. To effectively investigate the mentioned features in SACs/HEOs, several tools such as XRD, High -resolution transmission electron microscopy (HR-TEM), scanning transmission electron microscopy (STEM), energy dispersive spectroscopy (EDS or EDX), selected area electron diffraction (SAED), high annular angular dark field (HAADF) microscopy, inductive couple plasma (ICP), X-ray absorption near edge spectroscopy (XANES), EXAFS are judiciously used. The elaborate description of the scope and limitations of these techniques can be found in these recommended review articles [1,41,46,61].

Typically, XRD technique is very an important tool to elucidate the crystal structure of HEOs and to provide a clear distinction between single phase HEOs and multi-phased multielement oxides. Fundamentally, different metal oxides that makes up the HEO composition typically have different crystal structures. The goal is to crystallize such divergent structures into one crystal lattice. An implication of this is that the XRD pattern observed from the HEO must feature a diffraction pattern that matches only one crystal structure. Evidence of diffraction patterns corresponding to different crystal structures should be regarded as a phase segregation and such a compound is not entropy stabilized. For example, the first high entropy oxide synthesized consisted of Ni Cu, Mg, Zn, Co. Although Cu naturally crystallizes in a tenorite structure and Zn has a wurtzite structure, the final $(NiCuMgZnCo)O_x$ crystalizes into a single phase rocksalt structure without any tenorite or wurtzite phases [47,117]. However, it should be noted that sometimes, the final crystal structure of the HEOs would not reflect the structure of any one of the elements but crystalizes into a favourable phase to reflect the mixture. For an example, Fe, Co, Ni, Cr, Mn crystallizes into a single-phase HEO with NiFeOx type spinel structure [137].

Similar trend is observed for high entropy perovskite oxides where the final single-phase structure crystalizes into a typical perovskite oxide structure [93,138]. Furthermore, there are cases where formation of the HEO is motivated by the substitution of smaller cations into the crystal lattice of a larger cation. In such cases, it is thermodynamically favourable for the final HEOs to exhibit similar diffraction pattern with the larger individual elements. For example, partial substitution of ZrO_2 with Ni, Fe, Co, Mn and Cu to form $Zr_{0.5}(NiMnFeCoCu)O_x$ crystallizes into a Cubic ZrO_2 crystal structure. Similarly, high entropy $(CeHfZrSnEr)O_x$ crystallizes into a cubic CeO_2 structure without any other diffraction patterns [98]. It should be noted that in such cases where larger cations are substituted with smaller ones, shrinkage of the lattice may be observed and a resultant shift to higher than 2 theta is evident. Also, slight changes in unit cell volume, lattice parameters and even strain may evolve. To fully understand all these changes, it is recommended to carryout careful analysis of the resultant HEOs relative to an initial structural model. For such proposes, a comprehensive analysis such as Rietveld and microstrain analysis is required [45,97,105]. Complementary to the XRD, HR-TEM, SAED and STEM-EDS are necessary to probe deeper into the atomic arrangements (to identify defects), crystallization (polycrystallinity or monocrystallinity) and the unform distribution of constituent cations within the HEO structure respectively [47,97,98,105]. Another important analysis is the elemental ratio which is more reliably determined via ICP-MS or ICP-OES. Since equimolar ratio of cations within the HEO is a fundamental requirement for most HEOs (although nonstoichiometric HEOs exists), it is necessary to know the ratio of each cation relative to the other. Generally, for equimolar compositions, molar ratio should be close to unity within the limits of experimental errors.

4.2. Catalytic performances of SACs supported on HEOs

Pioneering efforts by Dai's group [104] paved a way for this emergent field of SACs stabilization on HEOs. In their early work, 0.3 wt% Pt single atoms were stabilized on high entropy $(NiMgCuZnCo)O_x$ to form the corresponding $Pt/(NiMgCuZnCo)O_x$ via co-precipitation followed by calcination at 900 °C. Prior to application for CO oxidation, the electronic structure of the Pt was modified from Pt^{4+} (O-Pt-O-M) to Pt^{2+} (Pt-O-M) via the reduction in hydrogen. Collectively, the incorporation of Pt into the $(NiMgCuZnCo)O_x$ system improved the catalytic performance. The as-synthesized $(NiMgCuZnCo)O_x$ has an onset temperature of about 160 °C with complete CO conversion at about 305 °C, significantly higher than the as-synthesized Pt/(NiMgCuZnCo)Ox with an onset temperature of about 100 °C and complete CO conversion at 245 °C. Further reduction of the $Pt/(NiMgCuZnCo)O_x$ dramatically improved the catalytic performance. The reduced 0.3 wt% $Pt/(NiMgCuZnCo)O_x$ has an onset temperature of 60 °C with 100% CO conversion at 155 °C. Based on these conversion temperatures and efficiencies, the activation energies for CO oxidation over the $(NiMgCuZnCo)O_x$, as-synthesized 0.3 wt% $Pt/(NiMgCuZnCo)O_x$ and reduced 0.3 wt% $Pt/(NiMgCuZnCo)O_x$ were 91.5, 57.2 and 54.8 kJ/mol respectively, highlighting the effect of electronic structure and coordination environment of SACs supported by HEOs on their superior catalytic performance.

In another study, using Ball-milling, Chen et al. [135] stabilized up to 5 wt% Pt and Ru in the form of single atoms and NPs (2–3 nm) on an HEO $(NiMgCuZnCo)O_x$ under ambient conditions and used the system for CO_2 hydrogenation (Fig. 11). The frictional and centrifugal force generated during the milling process was leveraged to create local environments sufficient to induce the formation of Pt/HEO or Ru/HEO without further calcination. The evolution of a single-phase HEO shows a direct relation with the milling time. Single phase HEO was achieved after 2 hours of milling without diffraction peaks corresponding to either Pt or Ru. To fully crystallize the matrix, 5 wt% Pt-HEO was sintered at 500 °C in the air for 2 hours. The 2 wt% and 5 wt% Ru and Pt-HEO calcined at 500 °C denoted as Ru-500 and Pt-500 were subjected to the catalytic reduction of CO_2. The 2 wt% Ru-500 and Pt-500 exhibited CO yields of 33.9% and 36.6% and CO_2 conversion of 40.1% and 43.4% respectively. Further increment in the Ru and Pt dispersions to 5 wt% significantly increased the catalytic performance, demonstrating a CO yield of 45.7% and 46.1% respectively with CO_2 conversion of 45.4% and 47.8%. The Pt-500 exhibited remarkable stability over 12 hours at high temperature [135].

Similarly, single Pd atoms were stabilized on an HEO $(CeZrHfTiLa)O_x$ (hereafter denoted as Pd@HEFO) via mechanochemical strategy [45], and used to catalyse CO oxidation. XANES confirms the presence of a Pd-O-M bond only indicating single palladium atoms (Fig. 12**A**).

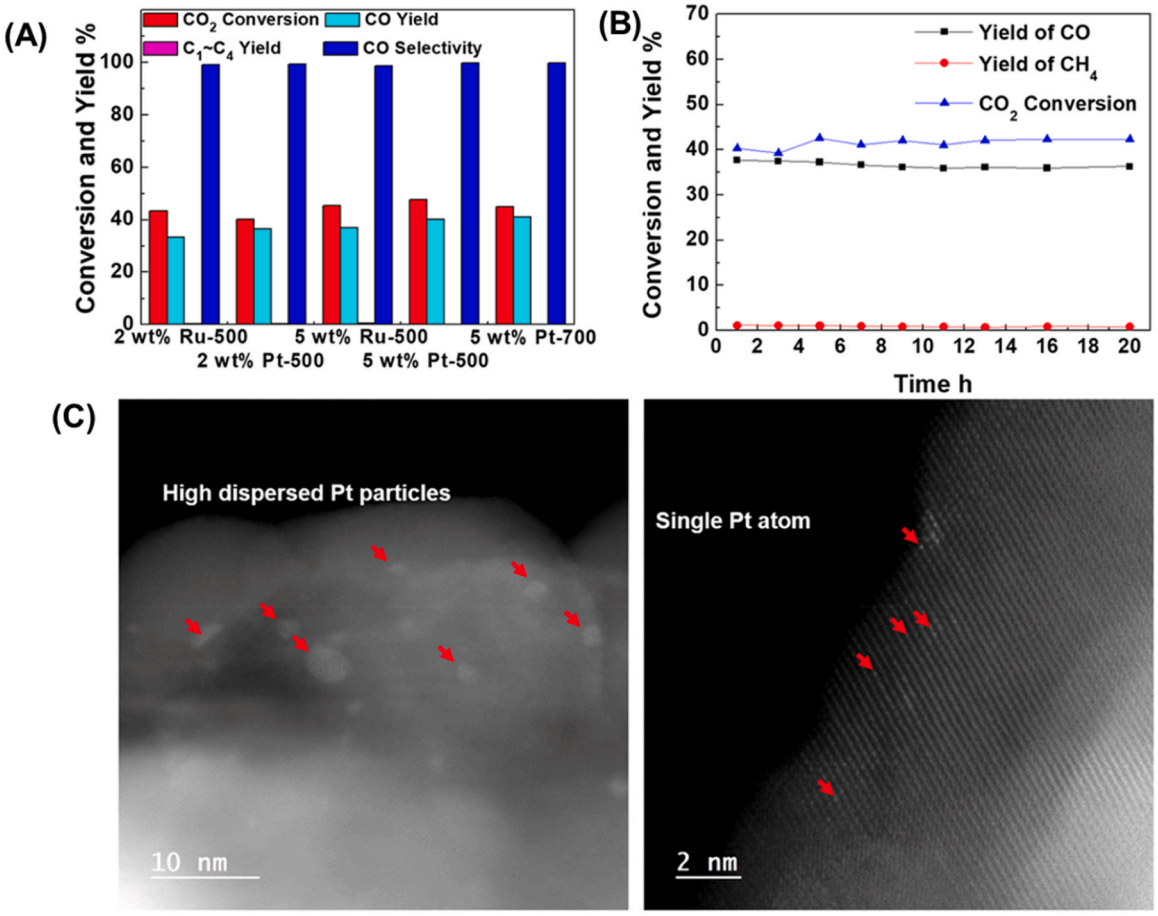

Fig. 11. (A) CO_2 hydrogenation activity of synthesized SACs/HEOs; 2 wt% Pt-500, 5 wt% Pt-500, 2 wt% Ru-500, and 5 wt% Ru-500 under 500°C reaction temperature, (B) CO_2 hydrogenation stability at 500 °Cover 5 wt% Pt-500, and (C) STEM result of 5 wt% Pt-500 after hydrogenation of CO_2 at 500 °C for 2 h [135].

Furthermore, diffraction patterns obtained from XRD showed a single-phase structure without additional diffraction peaks for palladium. Interestingly, a shift in 2 theta angle with an increasing amount of Pd (0.5 wt%-2wt%) was observed (Fig. 12**B**). The onset temperature for the high entropy (CeZrHfTiLa)O was 230 °C. However, upon the incorporation of 1 wt% Pd, the catalytic response dramatically improved with a lower onset temperature of 80 °C and completed CO conversion at 170 °C. Similar loading of palladium was supported on CeO_2 to form Pd@CeO_2. The catalytic response was less than that of the high entropy fluorite oxide (HEFO) $(CeZrHfTiLa)O_x$ without Pd, demonstrating an onset temperature of 223 °C and complete CO conversion at 253 °C. Evidently, Pd@HEFO exhibits lower activation energy for CO oxidation when compared to Pd@CeO_2 (Fig. 12**C**). The Pd@HEFO shows activity retention when subjected to hydrothermal treatment at 750 °C for 10 hours while significant activity loss was seen in palladium stabilized on CeO_2 (Pd@CeO_2) (Fig. 12D). This clearly demonstrates the superior nature of HEO supports compared to binary or low entropy metal oxide supports. This entails that the Pd atoms not only adsorb on the surface of $(CeZrHfTiLa)O_x$ but also are randomly substituted into the fluorite structure. Interestingly, Pd atoms stabilized on HEPO exhibited significantly higher oxygen vacancies (47.1%) than conventional CeO_2 Supports (24.7%) due to the high surface reducibility of HEOs.

To further highlight the unique role of entropic stabilizing, binary metal oxides were individually used as support for the Pd atoms. Unfortunately, in such binary systems, XRD peaks corresponding to Pd were observed at similar metal loadings showing somewhat aggregation into NPs and formation of multiphase. SACs stabilized on HEFO could be simultaneously anchored on the surface via Pd-O-M bond and within the bulk to form a $(Pd_yCeZrTiLa)O_x$ solid solution. Such solid solution formation is thermodynamically favoured, and entropy driven in HEOs. Conversely, Pd aggregation is observed when CeO_2 is used as the support where the thermodynamic landscape for solid solution formation is enthalpy controlled. This means that it is much easier to stabilize SACs within HEOs than conventional supports. Also, the surface lattice oxygen of HEOs is easily reducible compared. This clearly confirms that entropy driven effects within the HEO support promotes the stabilization of Pd atoms.

Via sonochemical strategy, Okejiri et al. [97] homogenously dispersed 0.2 wt% Ru into a HEPO (ABO_3) to form the corresponding high entropy $Ru_{0.13}/Ba_{0.3}Sr_{0.3}Bi_{0.4}(Zr_{0.2}Hf_{0.2}Ti_{0.2}Fe_{0.27})O_3$ hereafter referred to as Ru/HEPO-7, high entropy $Ba_{0.4}Sr_{0.4}Bi_{0.2}(Zr_{0.3}Hf_{0.3}Ti_{0.2}Fe_{0.2})O_3$ (hereafter referred to as HEPO-7) and low entropy $BaRuO_3$. This work exposes the possibility of obtaining high quality HEOs in a cheap and facile way while circumventing the calcination step. The catalytic activities of the synthesized systems towards CO oxidation were investigated with a central agender of understanding the role of entropy stabilization in enhancing catalytic activities. Ru-HEPO-7 containing only 0.2 wt% Ru shows 51% CO conversion at 90 °C with a retention time of one second (1 s). The $BaRuO_3$ having about 53 wt% Ru displays inferior catalytic relative to Ru/HEPO-7 with only 50% CO conversion at 255 °C. Furthermore, complete CO conversion was achieved over Ru/HEPO-7 at 118 °C while complete conversion could not be realized over the $BaRuO_3$ even at temperatures up to 300 °C. This trend is particularly interesting as Ru is considered as the main active sites for CO conversion. Intuitively, $BaRuO_3$ having more Ru loading should have higher catalytic performance. This opposite finding strongly supports the idea that entropic stabilization in entropy-oxide supports

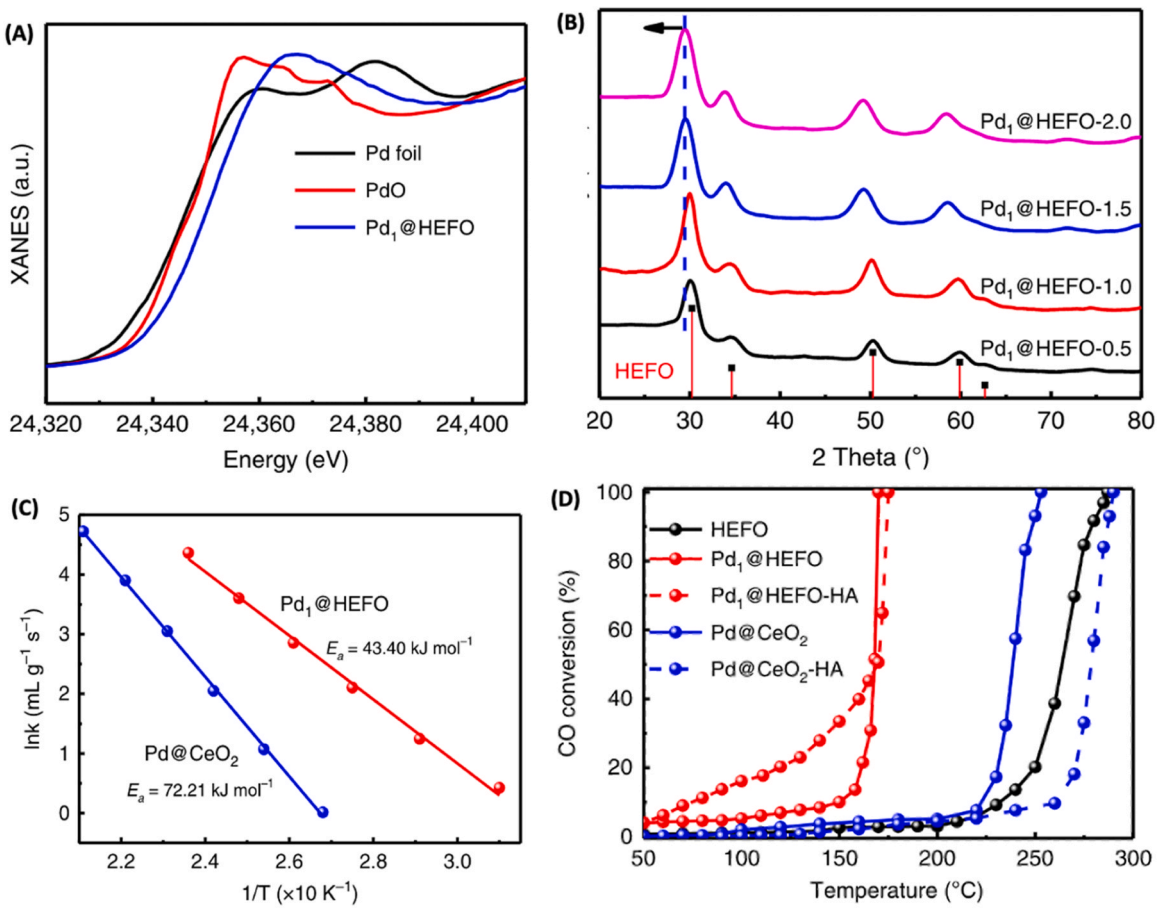

Fig. 12. (A) XANES spectra of Pd in Pd@HEFO showing the existence of Pd-O-M bond. (B) XRD spectra of Pd@HEFO with varying palladium loadings. Shift in 2 Theta with increasing palladium loadings. (C) Activation energies of Pd@HEFO and Pd@CeO_2 for CO oxidation. (D) Catalytic performance of HEFO, Pd@HEFO, Pd@CeO_2 under normal catalytic conditions as well as under has hydrothermal treatments at 750 ºC [45].

significantly reduces the activation barrier, leading to enhanced catalytic responses. On the other hand, HEPO-7 without any Ru did not display appreciable catalytic activity. Like findings by Xu et al. [45], noble metals stabilized on HEO supports have higher catalytic activities relative to bare HEOs and SACs supported on low entropy supports.

Furthermore, Chen et al. [139] explored the concept of temperature-dependent self-regenerative exsolution-dissolution, a phenomenon exclusive to perovskites [140] but now observed in HEOs [105], to stabilize 1 wt% Au, Pd, and Ru within HEO $(NiMgZnCuCo)O_x$. The Au/HEO was synthesized via a solid-state route followed by subsequent calcination at 900 °C. It is worth mentioning that the catalytic activities of these catalysts towards CO oxidation are affected by the exsolution-dissolution phenomena. The Au-HEO-700 having more surface Au particles demonstrated superior catalytic performance. The homogenous distribution of Au within the HEO and subsequent exsolution of Au to the surface at 700 °C was corroborated by STEM-EDS and XPS, showing increased intensity and agglomeration spots of Au particles. XRD patterns reveal the formation of single-phase Au/HEO without any impurity peaks. Upon calcination at a lower temperature (~700 °C), phase segregation occurs with distinct diffraction peaks corresponding to Au particles which reverted to the single-phase Au-HEO upon cyclic heating back to 900 °C. This interesting behaviour is conceptually conceived to prevent the agglomeration or sintering of catalytic active sites, especially for noble metals at high temperatures. Fig. 13 depicts

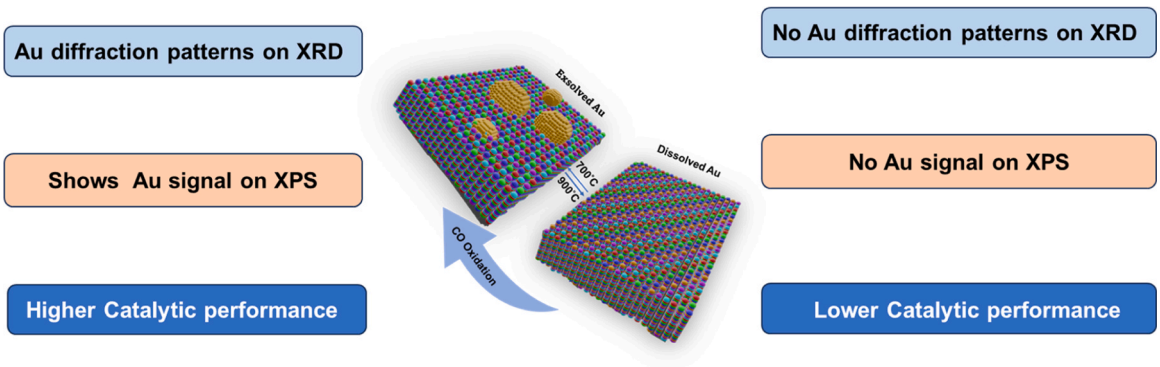

Fig. 13. (A) Regenerative exsolution-dissolution of Au in high entropy (MgNiCoCuZn) for CO oxidation. Adapted from [139].

the exsolution-dissolution of Au within HEO at different temperatures to form the correspondingAu-HEO-900 and Au-HEO-700. Evidently, Au/HEO calcined at 700 ºC demonstrated superior catalytic performance in CO oxidation due to larger surface concentration of the Au.

Via precise modulation of synthesis temperature, oxygen partial pressure, and configurational entropy, Li et al. [77] reported a new strategy to stabilize up to 10 different cations within the same crystal lattice, opening new possibilities for creating nanosized multi-element oxides (MEO) with rocksalt, fluorite and perovskite structures. This strategy has been experimentally and computationally verified in generating favourable phases when designing MEO of highly reducible metal oxides with low oxidative potential and stabilizing noble metals within the MEO matrix. Through this method, the denary high entropy metal oxide, $(ZrCe)_{0.6}(MgLaYHfTiCrMn)_{0.3}Pd_{0.1}O_{2-x}$ consisting of 10w% Pd was stabilized on electrospun carbon nanofibers. Their findings reveal that high configurational entropy is particularly important to stabilizing noble metals such as Pd within the MEO matrix while synthesis temperature and oxygen partial pressures are more important towards stabilizing cations with low oxidative potentials and easily reducible cations, respectively. To achieve this type of system, careful optimization of temperature, oxygen partial pressure, and number of constituent cations is very important. The synthesized denary nanostructure exhibited superior catalytic performance towards methane (CH_4) combustion compared to PdO_x and other quinary MEO synthesized via a similar protocol [77]. This presents a potential breakthrough over the limited SAC loadings achievable on HEOs.

Fig. 14(A-B) shows thermodynamic factors that drive single phase formation in multielement oxide systems, taking into perspective the chemical nature of the elements such as oxidation potentials, reduction potentials and noble metal stabilization. [77]. For easily oxidized metals, phase segregation occurs at lower temperatures. In addition, oxygen partial pressure affects single-phase formation in MEO containing highly reducible metals. Fundamentally, the single phase is driven by a highly oxidative environment (air). Similarly, high configurational entropy supports incorporation of Pd whereas phase segregation occurs at lower configurational entropy. Also, Fig. 10B clearly shows the role of high configurational entropy in stabilizing and enhancing the catalytic properties and stabilities of noble metals. As shown, PdOx stabilized on high entropy oxide consisting of 1 different cation (hereby denoted as 10-MEO) has the highest performance and stability. This implies the guided stabilization of noble metals on high entropy supports. Table 1 presents a list of representative SACs/HEO systems and their catalytic

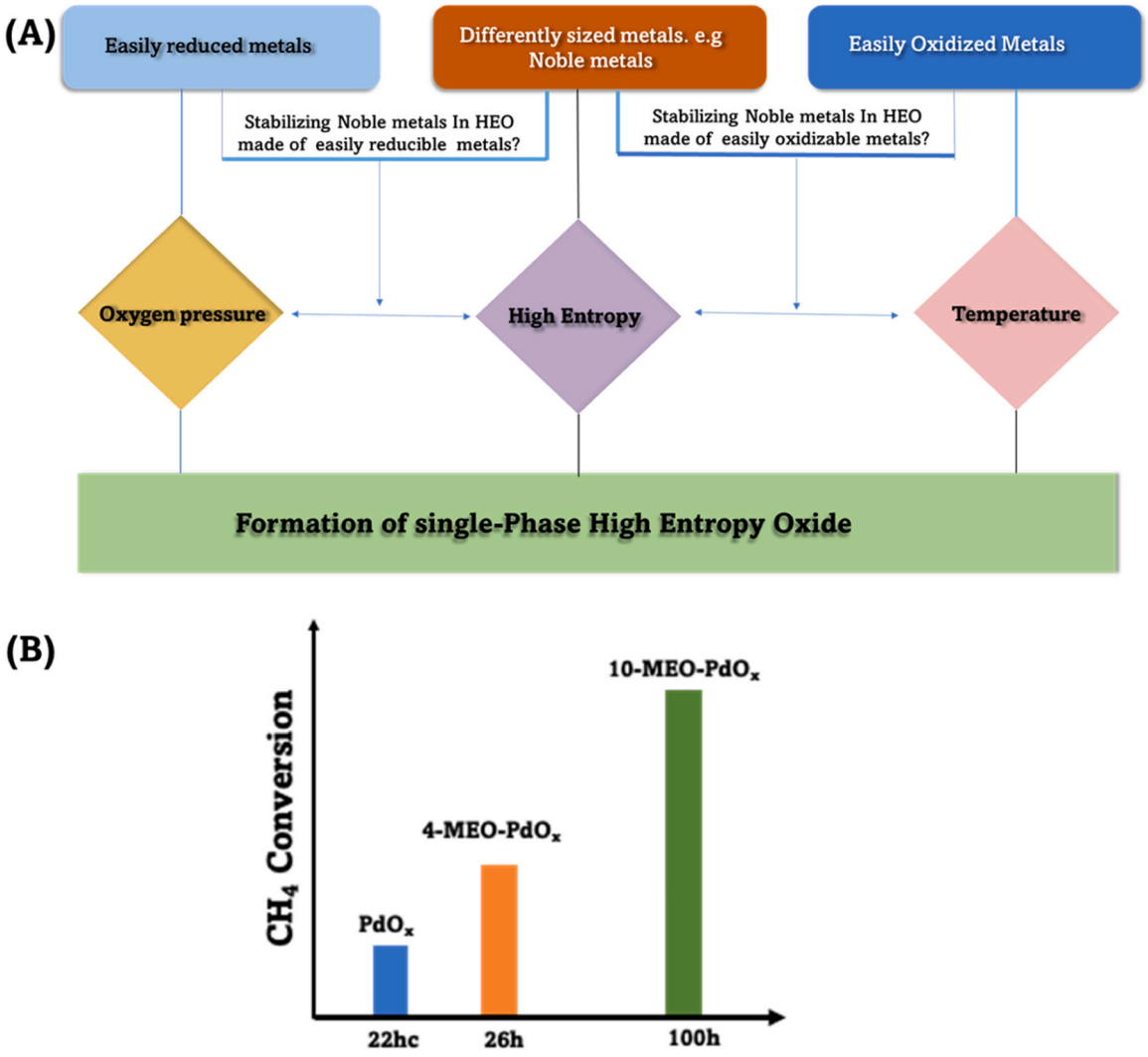

Fig. 14. (A) General design principles for multicomponent metal oxides and noble metal stabilization. Highlighting factors that most significantly affects single phase formation in relation to the intrinsic chemistry of cations selected. High oxygen partial pressure is required for easily reducible metals, high temperature for easily oxidizable metals, and a high configurational entropy supports the stabilization of noble metals. (B) CH_4 conversion performance and stabilities of unsupported PdO_x, PdO_x stabilized on low entropy oxide with 4 metals (4-MEO-PdO_x) and PdO_x stabilized on a denary HEO (10-MEO-PdO_x). Concept adapted from [77].

Table 1
A Summary of typical SACs/HEO systems and their catalytic applications and entropy driven behaviors.

System	Synthesis	Catalytic Performance	Notes	Ref
$Pd_1/(CeZrTiHfLa)O_x$ (0.5–2 wt% Pd)	Silica-templated mechanochemical strategy.	CO-Oxidation; $Pd_1/(CeZrTiHfLa)O_x$ Outperformed Pd_1/CeO_2 T_{onset} of ~80^0 C and 223^0 C respectively and T_{100} of 170^0 C and 253^0 C respectively.	High surface lattice oxygen reducibility, anti-sintering properties due to entropic stabilization.	[45]
$Pt/(NiMgCoCuZn)O_x$ (0.3 wt% Pt)	Co-deposition	CO-oxidation: chemical reactivity follows reduced $Pt/(NiMgCoCuZn)O_x$ > as-synthesized $Pt/(NiMgCoCuZn)O_x$ > $/(NiMgCoCuZn)O_x$. T_{100} of 155^0 C, 245^0 C and 305^0 C respectively.	Anti-sintering property due to entropic stabilization, favorable formation of Pt-O-M (Pt^{2+}) for CO oxidation.	[104]
$Pt/(NiMgCuZnCo)O_x$ (2 wt%, 5 wt%) $Ru//(NiMgCuZnCo)O_x$ (2 wt%, 5 wt%)	Ball milling	CO_2 hydrogenation: CO yield of 36.6% and 46.1% and CO_2 conversion of 43.4% and 47.8% for 2 wt% Pt and 5 wt% Pt under 500^0 C reaction condition respectively. CO yield of 33.9% and 45.7% for 2 wt Ru and 5 wt% Ru respectively. Also, CO_2 conversion was 40.1% and 45.4% for 2 wt Ru and 5 wt Ru respectively. Catalysts stable for 12 h under reaction at 500^0 C.	Anti-sintering with no capacity loss at high temperature due to entropic stabilization.	[135]
$Ru/(Ba_{0.4}Sr_{0.4}Bi_{0.2}(Zr_{0.3}Hf_{0.3}Ti_{0.2}Fe_{0.2})O_3$ (Ru/HEPO-7) (0.2 wt% Ru)	Ultrasonication	CO-Oxidation $Ru/(Ba_{0.4}Sr_{0.4}Bi_{0.2}(Zr_{0.3}Hf_{0.3}Ti_{0.2}Fe_{0.2})O_3$ (0.2 wt%Ru) (Ru/HEPO-7) outperformed $BaRuO_3$ (53 wt% Ru) and HEPO (0 wt Ru). Ru/HEPO-7 achieved 51% CO conversion in ~1 s at 90^0 C while $BaRuO_3$ achieved 50% conversion at ~255^0 C. T_{100} was 118^0 C for Ru/HEPO-7 while $BaRuO_3$ could not achieve 100% conversion even at temperatures > 300^0 C.	Excellent dispersion of Ru atoms within Ru/HEPO as compared to $BaRuO_3$ enabled by entropic stabilization of Ru.	[97]
$Pd/(CeHfZrSnEr)O_x$ (0.5–1 wt% Pd)	Ultrasonication	CO Oxidation: $Pd_{0.5}/(CeHfZrSnErO)_x$ and $Pd_1/(CeHfZrSnErO)_x$ demonstrate higher performance compared to Pd/CeO_2 or bare $(CeHfZrSnErO)_x$. catalysts reactivity follows the trend $Pd_1/(CeHfZrSnErO)_x \geq Pd_{0.5}/(CeHfZrSnErO)_x >> Pd_1/CeO_2 > (CeHfZrSnErO)_x > CeO_2$. $Pd_{0.5}/(CeHfZrSnErO)_x$ and $Pd_1/(CeHfZrSnErO)_x$ show the least onset temperature of ~50^0 C and ~70^0 C respectively with T_{100} of 140^0 C and 150^0 C respectively.	High surface Oxygen reducibility that leads to high oxygen vacancy concentration. Also, entropic stabilization that enhanced thermal and chemical stability leading to long term cycling performance.	[98]
$Pt\text{-}HEO/Al_2O_3$	Combined sol-gel followed by ball milling.	CO oxidation: Pt stabilized on HEO/Al_2O_3 shows higher performance than Pt-HEO or $Pt\text{-}Al_2O_3$. Pt- HEO/Al_2O_3 shows an onset temperature of 50^0 C and a decreased T_{100} of 180^0 C. for the different Pt-based systems, the activation energies for CO oxidation follows the trend Pt-HEO/Al_2O_3 (26.93 kJ/mol) < $Pt\text{-}Al_2O_3$(89.13 kJ/mol) < Pt-HEO (109.66 kJ/mol). No capacity loss was observed for Pt- HEO/Al_2O_3 up to 540 hours under reaction conditions and up to 10 hours with hydrothermal treatment at 750^0 C.	Interfacing HEO with Al_2O_3 led to the formation of oxygen vacancies and stabilization of isolated Pt species. Entropic stabilization affords Pt- HEO/Al_2O_3 with anti-sintering properties under hydrothermal conditions.	[141]
$Mo/(LaMnNiFeCoCu)O_x$ (0.35 wt% Mo)	Sacrificial Template -assisted protocol	Oxidation desulfurization: Mo dispersed on high entropy perovskite oxide (Mo/HEPO-SAC) exhibits better performance than Mo dispersed on low entropy perovskite oxde (Mo/LMO-SAC). (Mo/HEPO-SAC achived 100% oxidative conversion of dibenzothiophene in 1 hour.	Higher Mo dispersion, more oxygen vacancy and better redox properties. High cycling stability	[138]
$Rh/(MgNiCoCuZn)O_x$ (5 wt% Rh)	Nitrate-glycine combustion	CO_2 dehydrogenation: Rh stabilized on HEO had 99% CO selectivity during the CO_2 hydrogenation process. This is higher than selectivity achieved by Rh stabilized on single metal oxides that makes up the HEO. Cu-Zn synergy within the HEO promotes Metal-support interactions between Rh and HEO supports.	Formation of strong-metal support interaction between Rh and HEO support. Synergistic interference in HEO support optimizes CO adsorption energies.	[142]
$Au/(MgNiCuCoZn)O_x$ (1 wt% Au)	Ball milling	CO Oxidation: $Au/(MgNiCuCoZn)O_x$ calcined at 700 and 900 exhitied varying activity towards CO. catalysts exhited T_{50} at 218^0 C and 284^0 C respectively.	Catalysts exhibit reversible temperature dependent phase exsolution, enabled by unique entropic stabilization within the HEO support. Anti-sintering at elevated temperature.	[139]
$(ZrCe)_{0.6}(MgLaYHfTiCrMn)_{0.3}Pd_{0.1}O_{2-x}$ (10 wt% Pd)	Joule heating	CH_4 combustion: Pd stabilized within the denary high entropy oxide labelled as 10-MEO-Pd shows the highest performance compared to unsupported PdO_x or Pd stabilized on lower entropy systems. 10.MEO-Pd achieved Complete CH_4 conversion at 673 K. stability test shows 10-MEO-PdO_x > 4-MEO-PdO > PdO_x. 10-MEO-PdO_x had no capacity loss for up to 100 h as opposed to 4-MEO-PdO_x which experienced capacity drop from 31% to 20% in just 26 h. Unsupported PdOx was deactivated after 22 h.	High catalytic performance with extreme thermal stabilities, due to high configurational entropy.	[77]

performance due to entropic sbablizataion.

From the above case-studies, it can be deduced that a range of factors can contribute to the superior catalytic performances of SACs stabilized on HEOs. Primarily, entropic stabilization affords these single atoms with enhanced thermal and chemical stabilities that delay deactivation during reactions occurring under harsh conditions. Also. It has been shown that in the case of SACs stabilized on HEOs, the HEO support also participates in the chemical reaction therefore transcending performances exhibited by SACs on conventional binary metal oxides. Additionally, electronic interactions between cations in the support may favorability adjust the metal-support interactions between the single atoms and the HEO support, resulting in lower adsorbate binding

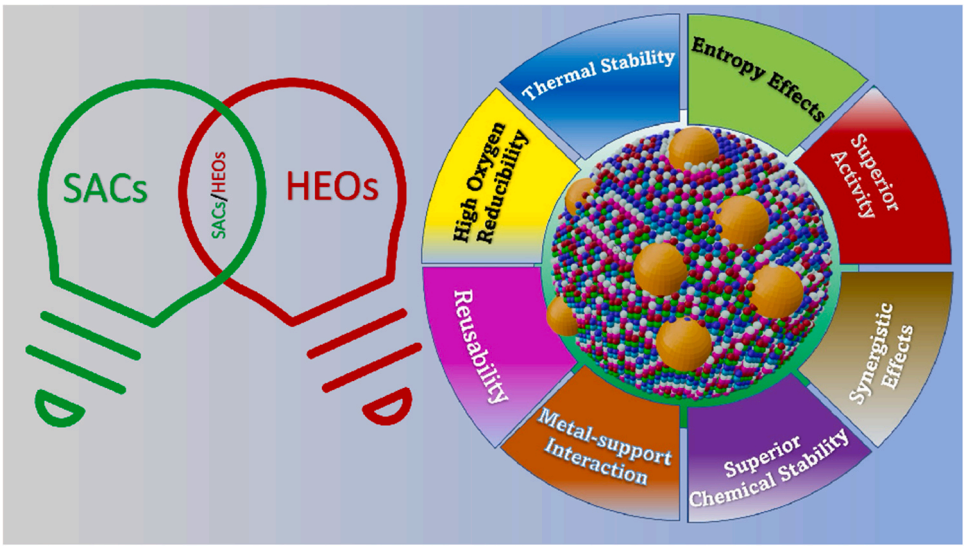

Fig. 15. Highlighted superior properties observed in SACs/HEOs.

energies, thus the activation energies. Fig. 15 outlines major attributes and advantages demonstrated by HEO supported SACs over SACs stabilized on conventional supports.

5. Summary

SAC has recently dominated the landscape of heterogenous catalysis research. More recent novelties are arising from the concept of entropic stabilization to engineer multicomponent metal oxide systems popularly known as HEOs. HEOs are multicationic oxide systems, consisting of five or more different cations stabilized into a single-phase crystal structure and collectively having a configurational entropy equal or greater than 1.5 R [90]. The compositional flexibility, diverse protocol for synthesis, unconventional catalytic activity and most importantly their superior chemical and thermal stabilities have motivated their widespread applications within the heterogenous catalyst domain.

In this review, we present a deliberate effort to emphasize the interactions of SACs with HEO supports, highlighting the synthesis protocols, unique stabilities, and unconventional catalytic behaviours during thermocatalytic processes such as CO oxidation, CO_2 reduction and CH_4 combustion. These reactions have been chosen to evaluate the catalytic behaviours of SACs/HEO because of the extreme conditions under which they occur, therefore speaking to the activity, selectivity, and stability of SACs/HEO.

We also discuss how the entropic effect in the HEOs supports induces unconventional behaviours and bolsters strong metal-support interactions to achieve optimal stabilities under harsh chemical or thermal conditions, which is particularly important to the applications of SACs on a commercial scale. Comparisons made in this review clearly show that SACs stabilized on HEO supports exhibit superior catalytic performance and stabilities, exceeding bare HEOs, SACs supported on conventional binary metal oxides, and unsupported noble metal oxides. We have highlighted principles and models, both theoretically derived and experimentally validated, that have been proven to be effective in achieving single-phase SACs/HEOs.

6. Future research and outlook

In the realm of HEOs, research has predominantly focused on uncovering the rules and principles governing the formation of single-phase structures. However, this emphasis has somewhat overshadowed a deeper exploration of the fundamental factors that influence their catalytic performance. This has led to an "availability-driven application scenario", where the research has largely been cantered to investigating the catalytic behaviors of already established HEOs for various processes. Fortunately, the current trends in HEO design have started to consider fundamental aspects that can significantly enhance their catalytic activities. These include techniques like defect engineering to increase oxygen vacancies, modified synthesis protocols to achieve higher surface areas, and the incorporation of highly active noble metals as NPs or single atoms. Looking ahead, we anticipate a shift towards a more application-driven approach to HEO development, with the desired applications guiding the design process.

Despite the recent progress, we still lack a comprehensive understanding of the metal-support interaction within HEO-supported SACs. This understanding is crucial for achieving a tuneable coordination environment and electronic structure for the stabilized SACs. Given the complexity of HEO supports, this may prove challenging. Given the early stage of this field, it is essential to explore how various fundamental aspects of different HEO systems, such as crystal structure, cation composition, configurational entropy, oxygen vacancies, charge distortion, and valence mismatch, impact the stability, selectivity, and activity of stabilized SACs. For example, the choice of cations in the HEO lattice can have a profound impact on the catalytic performance. Varying cation compositions can affect the electronic structure, charge distribution, and binding energy of SACs. It's important to select cations that enhance the interaction between SACs and the HEO support, improving stability and catalytic activity. The presence of oxygen vacancies in HEOs can promote the adsorption of reactants and the mobility of reactant species. Oxygen vacancies can serve as active sites for catalytic reactions and play a role in enhancing the catalytic activity of SACs. Therefore, careful control of the density and distribution of oxygen vacancies is critical for optimizing catalytic performance. To impact the stability, selectivity, and activity of stabilized SACs, researchers should conduct systematic studies to optimize each of these factors in the context of their specific catalytic applications. Understanding the interplay between these parameters and their effects on SACs' performance is essential for designing HEO-supported catalysts with enhanced catalytic properties. It may require a combination of theoretical modelling, advanced characterization techniques, and tailored synthesis methods to achieve the desired results.

Meanwhile, establishing systematic criteria and principles for selecting suitable HEO supports is paramount for tailoring catalytic activity, maximizing stability, enhancing selectivity, optimizing electronic

and surface properties, minimizing side reactions, targeting resource efficiency, and standardizing research and development in the field of catalysis. By systematically evaluating HEO compositions and structures, researchers can make informed choices, leading to more efficient, stable, and selective catalytic systems while considering environmental and economic factors, ultimately advancing the practical application of HEOs in various industries.

Finally, there is a need for the development of flexible, cost-effective, and straightforward synthesis protocols that allow for reasonable SAC loading on HEO supports. The current synthesis protocols for SACs/HEOs primarily rely on a limited set of techniques, including mechanochemistry, co-deposition, joule heating, and sonochemistry. While these methods have shown promise, there is room for further improvement and diversification in the synthesis techniques. Some key considerations for expanding the synthesis options can be included but not limited to:

1. Diversification of Synthesis Techniques: In addition to the existing methods, researchers should explore and adapt other well-established synthesis techniques, such as sol-gel methods, atomic layer deposition (ALD), chemical vapor deposition (CVD), and hydrothermal synthesis. Each of these techniques has its unique advantages and can potentially provide more versatile options for the stabilization of SACs on HEO supports.
2. Optimization for Scalability and Cost-Effectiveness: It's essential to develop synthesis methods that are not only effective on a laboratory scale but also scalable for industrial applications. Scalability is crucial for the practical implementation of SACs/HEOs in real-world catalytic processes. Meanwhile, cost remains a significant concern in catalyst development. Research should focus on making the synthesis process cost-effective by using readily available, low-cost materials and minimizing the use of expensive or rare components.
3. Multi-scale Analysis Techniques: As new synthesis methods are developed; complementary characterization techniques should also be advanced. These techniques are essential for monitoring the quality and consistency of SAC loading and for understanding the resulting catalytic properties. At the nanoscale, HR-TEM and STEM reveal the atomic structure of SACs, affirming their single-atom nature, and offer insights into their coordination with HEO supports. This detailed structural information is crucial for understanding the fundamental properties of SACs. Moving to the microscale, X-ray Absorption Spectroscopy (XAS) provides insights into the local coordination environment of the metal atoms, revealing oxidation states and bond distances. Additionally, XPS characterizes the surface chemistry of the catalyst, which is vital for understanding its reactivity. On a larger scale, techniques such as XRD assess the influence of SACs on the structural properties of HEO supports. This information helps confirm the stability of the support material, which is critical for long-term catalytic applications. Further up the scale, surface area analysis (BET) measures the specific surface area, providing a mesoscale view and an indicator of potential catalytic activity. Thermal Analysis (TGA/DSC) at the millimeter scale evaluates the thermal stability of SACs/HEOs, ensuring that the catalysts can withstand the temperature conditions encountered during catalytic reactions. At the macroscale, electrochemical characterization methods like cyclic voltammetry and electrochemical impedance spectroscopy test the electrocatalytic performance of the materials, which is essential for understanding their behavior in real-world applications. In sum, multi-scale analysis allows researchers to obtain a deep understanding of the structure, composition, and behavior of SACs/HEOs, ultimately leading to the fine-tuning of catalyst design and optimization across different scales. This holistic approach is pivotal in unlocking the full potential of SACs/HEOs for sustainable and efficient catalytic processes, propelling catalysis into a new era of innovation and application.

In summary, the development of flexible, cost-effective, and straightforward synthesis protocols for SACs/HEOs is crucial for the practical application of these materials in catalysis. Diversifying synthesis techniques, optimizing for scalability, controlling loading, considering cost and environmental impact, and fostering interdisciplinary collaboration are all essential steps in advancing this field and harnessing the full potential of SACs supported by High Entropy Oxides.

CRediT authorship contribution statement

Panesun Tukur: Conceptualization, Investigation, Writing – original draft; **Frank Tukur**: Writing – review and editing; **Yirong Mo**: Writing – review and editing. **Qiangu Yan**: Writing – review and editing. **Chaochao Dun**: Writing – review and editing. **Jianjun Wei**: Conceptualization, Writing – review and editing, Funding, Supervision.

Declaration of Competing Interest

The authors declare that they have no known competing financial interests or personal relationships that could have appeared to influence the work reported in this paper.

Acknowledgments

This work was partially supported by US NSF (1832143) and NC state funding through the Joint School of Nanoscience and Nanoengineering (JSNN), UNCG. This work was performed at the JSNN, a member of Southeastern Nanotechnology Infrastructure Corridor (SENIC) and National Nanotechnology Coordinated Infrastructure (NNCI), which is supported by the National Science Foundation (ECCS-2025462).

References

[1] F. Zhang, Y. Zhu, H. Wang, Q. Lin, L. Zhang, X. Zhang, Noble-metal single-atoms in thermocatalysis, electrocatalysis, and photocatalysis, Energy Environ. Sci. 14 (2021) 2954–3009, https://doi.org/10.1039/d1ee00247c.
[2] L. Li, P. Wang, Q. Shao, X. Huang, Metallic nanostructures with low dimensionality for electrochemical water splitting, Chem. Soc. Rev. 49 (10) (2020) 3072–3106, https://doi.org/10.1039/d0cs00013b.
[3] Y. Zhang, Y. Mo, Z. Cao, Rational design of main group metal-embedded nitrogen-doped carbon materials as frustrated lewis pair catalysts for CO_2 hydrogenation to formic acid, ACS Appl. Mater. Interfaces 14 (1) (2022) 1002–1014, https://doi.org/10.1021/acsami.1c20230.
[4] C.R. Schwalm, S. Glendon, P.B. Duffy, RCP8.5 tracks cumulative CO2 emissions, Proc. Natl. Acad. Sci. U. S. A. 117 (33) (2020) 19656–19657, https://doi.org/10.1073/PNAS.2007117117.
[5] S. Hsiang, R. Kopp, A. Jina, J. Rising, M. Delgado, S. Mohan, D.J. Rasmussen, R. Muir-Wood, P. Wilson, M. Oppenheimer, K. Larsen, T. Houser, Estimating economic damage from climate change in the United States, Science 356 (6345) (2017) 1362–1369, https://doi.org/10.1126/science.aal4369.
[6] M. Burke, S.M. Hsiang, E. Miguel, Global non-linear effect of temperature on economic production, Nature 527 (7577) (2015) 235–239, https://doi.org/10.1038/nature15725.
[7] C. Wang, H. Shang, Y. Wang, H. Xu, J. Li, Y. Du, Interfacial electronic structure modulation enables CoMoOx/CoOx/RuOxto boost advanced oxygen evolution electrocatalysis, J. Mater. Chem. A 9 (25) (2021) 14601–14606, https://doi.org/10.1039/d1ta01226f.
[8] L. Zhou, R. Lv, Rational catalyst design and interface engineering for electrochemical CO2 reduction to high-valued alcohols, J. Energy Chem. 70 (2022) 310–331, https://doi.org/10.1016/j.jechem.2022.02.033.
[9] C. Wan, X. Duan, Y. Huang, Molecular design of single-atom catalysts for oxygen reduction reaction, Adv. Energy Mater. 10 (14) (2020) 1903815, https://doi.org/10.1002/aenm.201903815.
[10] X.W. Guo, S.M. Chen, H.J. Wang, Z.M. Zhang, H. Lin, L. Song, T.B. Lu, Single-atom molybdenum immobilized on photoactive carbon nitride as efficient photocatalysts for ambient nitrogen fixation in pure water, J. Mater. Chem. A 7 (34) (2019) 19831–19837, https://doi.org/10.1039/c9ta06653e.
[11] X. Jin, R. Wang, L. Zhang, R. Si, M. Shen, M. Wang, J. Tian, J. Shi, Electron configuration modulation of nickel single atoms for elevated photocatalytic hydrogen evolution, Angew. Chem. Int. Ed. 59 (17) (2020) 6894–6898, https://doi.org/10.1002/anie.201914565.
[12] B. Xia, Y. Zhang, J. Ran, M. Jaroniec, S.Z. Qiao, Single-atom photocatalysts for emerging reactions, ACS Cent. Sci. 7 (1) (2021) 39–54, https://doi.org/10.1021/acscentsci.0c01466.

[13] X. Li, W. Bi, L. Zhang, S. Tao, W. Chu, Q. Zhang, Y. Luo, C. Wu, Y. Xie, Single-atom Pt as Co-catalyst for enhanced photocatalytic H2evolution, Adv. Mater. 28 (12) (2016) 2427–2431, https://doi.org/10.1002/adma.201505281.

[14] Y. Chen, S. Ji, C. Chen, Q. Peng, D. Wang, Y. Li, Single-atom catalysts: synthetic strategies and electrochemical applications, Joule 2 (7) (2018) 1242–1264, https://doi.org/10.1016/j.joule.2018.06.019.

[15] L. Peng, L. Shang, T. Zhang, G.I.N. Waterhouse, Recent advances in the development of single-atom catalysts for oxygen electrocatalysis and zinc–air batteries, Adv. Energy Mater. 10 (2020) 2003018, https://doi.org/10.1002/aenm.202003018.

[16] Z. Song, Y.N. Zhu, H. Liu, M.N. Banis, L. Zhang, J. Li, K. Doyle-Davis, R. Li, T. K. Sham, L. Yang, A. Young, G.A. Botton, L.M. Liu, X. Sun, Engineering the low coordinated Pt single atom to achieve the superior electrocatalytic performance toward oxygen reduction, Small 16 (43) (2020) 2003096, https://doi.org/10.1002/smll.202003096.

[17] K. Maiti, S. Maiti, M.T. Curnan, H.J. Kim, J.W. Han, Engineering single atom catalysts to tune properties for electrochemical reduction and evolution reactions, Adv. Energy Mater. 11 (38) (2021) 2101670, https://doi.org/10.1002/aenm.202101670.

[18] L. Silvioli, A. Winiwarter, S.B. Scott, I.E. Castelli, P.G. Moses, I. Chorkendorff, B. Seger, J. Rossmeisl, Rational catalyst design for higher propene partial electro-oxidation activity by alloying Pd with Au, J. Phys. Chem. C. 126 (34) (2022) 14487–14499, https://doi.org/10.1021/acs.jpcc.1c10095.

[19] L. Shi, Y. Yin, S. Wang, H. Sun, Rational Catalyst Design for N2 reduction under ambient conditions: strategies toward enhanced conversion efficiency, ACS Catal. 10 (12) (2020) 6870–6899, https://doi.org/10.1021/acscatal.0c01081.

[20] Z.W. Chen, L.X. Chen, C.C. Yang, Q. Jiang, Atomic (single, double, and triple atoms) catalysis: Frontiers, opportunities, and challenges, J. Mater. Chem. A 7 (8) (2019) 3492–3515, https://doi.org/10.1039/c8ta11416a.

[21] X. Li, H. Rong, J. Zhang, D. Wang, Y. Li, Modulating the local coordination environment of single-atom catalysts for enhanced catalytic performance, Nano Res. 13 (7) (2020) 1842–1855, https://doi.org/10.1007/s12274-020-2755-3.

[22] S.A. Cook, A.S. Borovik, Molecular designs for controlling the local environments around metal ions, Acc. Chem. Res. 48 (8) (2015) 2407–2414, https://doi.org/10.1021/acs.accounts.5b00212.

[23] R. Ye, T.J. Hurlburt, K. Sabyrov, S. Alayoglu, G.A. Somorjai, Molecular catalysis science: Perspective on unifying the fields of catalysis, Proc. Natl. Acad. Sci. U. S. A. 113 (19) (2016) 5159–5166, https://doi.org/10.1073/pnas.1601766113.

[24] Y. Zhang, J. Yang, R. Ge, J. Zhang, J.M. Cairney, Y. Li, M. Zhu, S. Li, W. Li, The effect of coordination environment on the activity and selectivity of single-atom catalysts, Coord. Chem. Rev. 461 (2022) 214493, https://doi.org/10.1016/j.ccr.2022.214493.

[25] H. Zhang, G. Liu, L. Shi, J. Ye, Single-atom catalysts: emerging multifunctional materials in heterogeneous catalysis, Adv. Energy Mater. 8 (1) (2018) 1701343, https://doi.org/10.1002/aenm.201701343.

[26] A.J. Medford, A. Vojvodic, J.S. Hummelshøj, J. Voss, F. Abild-Pedersen, F. Studt, T. Bligaard, A. Nilsson, J.K. Nørskov, From the Sabatier principle to a predictive theory of transition-metal heterogeneous catalysis, J. Catal. 328 (2015) 36–42, https://doi.org/10.1016/j.jcat.2014.12.033.

[27] A. Corma, P. Concepción, M. Boronat, M.J. Sabater, J. Navas, M.J. Yacaman, E. Larios, A. Posadas, M.A. López-Quintela, D. Buceta, E. Mendoza, G. Guilera, A. Mayoral, Exceptional oxidation activity with size-controlled supported gold clusters of low atomicity, Nat. Chem. 5 (9) (2013) 775–781, https://doi.org/10.1038/nchem.1721.

[28] S. Mitchell, E. Vorobyeva, J. Pérez-Ramírez, The multifaceted reactivity of single-atom heterogeneous catalysts, Angew. Chem. Int. Ed. 57 (47) (2018) 15316–15329, https://doi.org/10.1002/ange.201806936.

[29] M.J. Walsh, K. Yoshida, A. Kuwabara, M.L. Pay, P.L. Gai, E.D. Boyes, On the structural origin of the catalytic properties of inherently strained ultrasmall decahedral gold nanoparticles, Nano Lett. 12 (4) (2012) 2027–2031, https://doi.org/10.1021/nl300067q.

[30] H. Mistry, A.S. Varela, S. Kühl, P. Strasser, B.R. Cuenya, Nanostructured electrocatalysts with tunable activity and selectivity, Nat. Rev. Mater. 1 (2016) 16009, https://doi.org/10.1038/natrevmats.2016.9.

[31] H. Mistry, R. Reske, Z. Zeng, Z.J. Zhao, J. Greeley, P. Strasser, B.R. Cuenya, Exceptional size-dependent activity enhancement in the electroreduction of CO2 over Au nanoparticles, J. Am. Chem. Soc. 136 (47) (2014) 16473–16476, https://doi.org/10.1021/ja508879j.

[32] Q. Sun, N. Wang, T. Zhang, R. Bai, A. Mayoral, P. Zhang, Q. Zhang, O. Terasaki, J. Yu, Zeolite-encaged single-atom rhodium catalysts: highly-efficient hydrogen generation and shape-selective tandem hydrogenation of nitroarenes, Angew. Chem. Int. Ed. 58 (51) (2019) 18570–18576, https://doi.org/10.1002/anie.201912367.

[33] B. Qiao, A. Wang, X. Yang, L.F. Allard, Z. Jiang, Y. Cui, J. Liu, J. Li, T. Zhang, Single-atom catalysis of CO oxidation using Pt1/FeOx, Nat. Chem. 3 (8) (2011) 634–641, https://doi.org/10.1038/nchem.1095.

[34] A. Bakandritsos, R.G. Kadam, P. Kumar, G. Zoppellaro, M. Medved, J. Tuček, T. Montini, O. Tomanec, P. Andrýsková, B. Drahoš, R.S. Varma, M. Otyepka, M. B. Gawande, P. Fornasiero, R. Zbořil, Mixed-valence single-atom catalyst derived from functionalized graphene, Adv. Mater. 31 (17) (2019) 1900323, https://doi.org/10.1002/adma.201900323.

[35] X. Li, A.E. Surkus, J. Rabeah, M. Anwar, S. Dastigir, H. Junge, A. Brückner, M. Beller, Cobalt single-atom catalysts with high stability for selective dehydrogenation of formic acid, Angew. Chem. Int. Ed. 59 (37) (2020) 15849–15854, https://doi.org/10.1002/anie.202004125.

[36] Z. Li, Y. Chen, S. Ji, Y. Tang, W. Chen, A. Li, J. Zhao, Y. Xiong, Y. Wu, Y. Gong, T. Yao, W. Liu, L. Zheng, J. Dong, Y. Wang, Z. Zhuang, W. Xing, C.T. He, C. Peng, W.C. Cheong, Q. Li, M. Zhang, Z. Chen, N. Fu, X. Gao, W. Zhu, J. Wan, J. Zhang, L. Gu, S. Wei, P. Hu, J. Luo, J. Li, C. Chen, Q. Peng, X. Duan, Y. Huang, X.M. Chen, D. Wang, Y. Li, Iridium single-atom catalyst on nitrogen-doped carbon for formic acid oxidation synthesized using a general host–guest strategy, Nat. Chem. 12 (8) (2020) 764–772, https://doi.org/10.1038/s41557-020-0473-9.

[37] O.Y. Podyacheva, D.A. Bulushev, A.N. Suboch, D.A. Svintsitskiy, A.S. Lisitsyn, E. Modin, A. Chuvilin, E.Y. Gerasimov, V.I. Sobolev, V.N. Parmon, Highly stable single-atom catalyst with ionic Pd active sites supported on n-doped carbon nanotubes for formic acid decomposition, ChemSusChem 11 (21) (2018) 3724–3727, https://doi.org/10.1002/cssc.201801679.

[38] P. Kumar, K. Kannimuthu, A.S. Zeraati, S. Roy, X. Wang, X. Wang, S. Samanta, K. A. Miller, M. Molina, D. Trivedi, J. Abed, M.A. Campos Mata, H. Al-Mahayni, J. Baltrusaitis, G. Shimizu, Y.A. Wu, A. Seifitokaldani, E.H. Sargent, P.M. Ajayan, J. Hu, M.G. Kibria, High-density cobalt single-atom catalysts for enhanced oxygen evolution reaction, J. Am. Chem. Soc. 145 (14) (2023) 8052–8063, https://doi.org/10.1021/jacs.3c00537.

[39] H. Xu, Y. Zhao, Q. Wang, G. He, H. Chen, Supports promote single-atom catalysts toward advanced electrocatalysis, Coord. Chem. Rev. 451 (2022) 214261, https://doi.org/10.1016/j.ccr.2021.214261.

[40] H. Wei, K. Huang, D. Wang, R. Zhang, B. Ge, J. Ma, B. Wen, S. Zhang, Q. Li, M. Lei, C. Zhang, J. Irawan, L.M. Liu, H. Wu, Iced photochemical reduction to synthesize atomically dispersed metals by suppressing nanocrystal growth, Nat. Commun. 8 (2017) 1490, https://doi.org/10.1038/s41467-017-01521-4.

[41] R. Lang, X. Du, Y. Huang, X. Jiang, Q. Zhang, Y. Guo, K. Liu, B. Qiao, A. Wang, T. Zhang, Single-Atom Catalysts Based on the Metal-Oxide Interaction, Chem. Rev. 120 (21) (2020) 11986–12043, https://doi.org/10.1021/acs.chemrev.0c00797.

[42] Z.X. Wei, Y.T. Zhu, J.Y. Liu, Z.C. Zhang, W.P. Hu, H. Xu, Y.Z. Feng, J.M. Ma, Recent advance in single-atom catalysis, Rare Met 40 (4) (2021) 767–789, https://doi.org/10.1007/s12598-020-01592-1.

[43] Y. Zhang, J. Zhao, H. Wang, B. Xiao, W. Zhang, X. Zhao, T. Lv, M. Thangamuthu, J. Zhang, Y. Guo, J. Ma, L. Lin, J. Tang, R. Huang, Q. Liu, Single-atom Cu anchored catalysts for photocatalytic renewable H2 production with a quantum efficiency of 56%, Nat. Commun. 13 (2022) 58, https://doi.org/10.1038/s41467-021-27698-3.

[44] T.X. Nguyen, Y.C. Liao, C.C. Lin, Y.H. Su, J.M. Ting, Advanced high entropy perovskite oxide electrocatalyst for oxygen evolution reaction, Adv. Funct. Mater. 31 (27) (2021) 2101632, https://doi.org/10.1002/adfm.202101632.

[45] H. Xu, Z. Zhang, J. Liu, H. Chen, S. Xu, Q. Lin, Y. Jiao, J. Wang, Y. Wang, Y. Chen, S. Dai, Entropy-stabilized single-atom Pd catalysts via high-entropy fluorite oxide supports, Nat. Commun. 11 (2020) 3908.

[46] G.M. Tomboc, X. Zhang, S. Choi, D. Kim, L.Y.S. Lee, K. Lee, Stabilization, characterization, and electrochemical applications of high-entropy oxides: critical assessment of crystal phase–properties relationship, Adv. Funct. Mater. 32 (43) (2022) 2205142, https://doi.org/10.1002/adfm.202205142.

[47] C.M. Rost, E. Sachet, T. Borman, A. Moballegh, E.C. Dickey, D. Hou, J.L. Jones, S. Curtarolo, J.P. Maria, Entropy-stabilized oxides, Nat. Commun. 6 (2015) 8485, https://doi.org/10.1038/ncomms9485.

[48] J.W. Yeh, S.K. Chen, S.J. Lin, J.Y. Gan, T.S. Chin, T.T. Shun, C.H. Tsau, S. Y. Chang, Nanostructured high-entropy alloys with multiple principal elements: novel alloy design concepts and outcomes, Adv. Eng. Mater. 6 (5) (2004) 299–303, https://doi.org/10.1002/adem.200300567.

[49] A. Sarkar, Q. Wang, A. Schiele, M.R. Chellali, S.S. Bhattacharya, D. Wang, T. Brezesinski, H. Hahn, L. Velasco, B. Breitung, High-entropy oxides: fundamental aspects and electrochemical properties, Adv. Mater. 31 (26) (2019) 1806236, https://doi.org/10.1002/adma.201806236.

[50] M. Naguib, M. Kurtoglu, V. Presser, J. Lu, J. Niu, M. Heon, L. Hultman, Y. Gogotsi, M.W. Barsoum, Two-dimensional nanocrystals produced by exfoliation of Ti 3AlC 2, Adv. Mater. 23 (37) (2011) 4248–4253, https://doi.org/10.1002/adma.201102306.

[51] B. Cantor, I.T.H. Chang, P. Knight, A.J.B. Vincent, Microstructural development in equiatomic multicomponent alloys, Mater. Sci. Eng. A 375-377 (2004) 213–218, https://doi.org/10.1016/j.msea.2003.10.257.

[52] Y. Ma, Y. Ma, Q. Wang, S. Schweidler, M. Botros, T. Fu, H. Hahn, T. Brezesinski, B. Breitung, High-entropy energy materials: challenges and new opportunities, Energy Environ. Sci. 14 (5) (2021) 2883–2905, https://doi.org/10.1039/d1ee00505g.

[53] D.B. Miracle, O.N. Senkov, A critical review of high entropy alloys and related concepts, Acta Mater. 122 (2017) 448–511, https://doi.org/10.1016/j.actamat.2016.08.081.

[54] X. Wang, W. Guo, Y. Fu, High-entropy alloys: emerging materials for advanced functional applications, J. Mater. Chem. A 9 (2) (2021) 663–701, https://doi.org/10.1039/d0ta09601f.

[55] A. Sarkar, L. Velasco, D. Wang, Q. Wang, G. Talasila, L. de Biasi, C. Kübel, T. Brezesinski, S.S. Bhattacharya, H. Hahn, B. Breitung, High entropy oxides for reversible energy storage, Nat. Commun. 9 (2018) 3400, https://doi.org/10.1038/s41467-018-05774-5.

[56] J.W. Yeh, Alloy design strategies and future trends in high-entropy alloys, JOM 65 (12) (2013) 1759–1771, https://doi.org/10.1007/s11837-013-0761-6.

[57] S. Wei, S.J. Kim, J. Kang, Y. Zhang, Y. Zhang, T. Furuhara, E.S. Park, C.C. Tasan, Natural-mixing guided design of refractory high-entropy alloys with as-cast tensile ductility, Nat. Mater. 19 (2020) 1175–1181, https://doi.org/10.1038/s41563-020-0750-4.

[58] S.S. Nene, M. Frank, K. Liu, S. Sinha, R.S. Mishra, B.A. McWilliams, K.C. Cho, Corrosion-resistant high entropy alloy with high strength and ductility, Scr. Mater. 166 (2019) 168–172, https://doi.org/10.1016/j.scriptamat.2019.03.028.

[59] M.G. Poletti, G. Fiore, F. Gili, D. Mangherini, L. Battezzati, Development of a new high entropy alloy for wear resistance: FeCoCrNiW0.3 and FeCoCrNiW0.3 + 5 at % of C, Mater. Des. 115 (2017) 247–254, https://doi.org/10.1016/j.matdes.2016.11.027.

[60] B.L. Musicó, D. Gilbert, T.Z. Ward, K. Page, E. George, J. Yan, D. Mandrus, V. Keppens, The emergent field of high entropy oxides: design, prospects, challenges, and opportunities for tailoring material properties, APL Mater. 8 (2020) 040912, https://doi.org/10.1063/5.0003149.

[61] Y. Sun, S. Dai, High-entropy materials for catalysis: a new frontier, Sci. Adv. (2021).

[62] S. Akrami, P. Edalati, M. Fuji, K. Edalati, High-entropy ceramics: review of principles, production and applications, Mater. Sci. Eng. R. Rep. 146 (2021) 100644, https://doi.org/10.1016/j.mser.2021.100644.

[63] R.Z. Zhang, M.J. Reece, Review of high entropy ceramics: design, synthesis, structure and properties, J. Mater. Chem. A 7 (2019) 22148–22162, https://doi.org/10.1039/c9ta05698j.

[64] Y. Chen, Z.W. Dai, J.Z. Jiang, High entropy metallic glasses: glass formation, crystallization and properties, J. Alloy. Compd. 866 (2021) 158852, https://doi.org/10.1016/j.jallcom.2021.158852.

[65] Z. Fan, H. Wang, Y. Wu, X. Liu, Z. Lu, Thermoelectric performance of PbSnTeSe high-entropy alloys, Mater. Res. Lett. 5 (3) (2017) 187–194, https://doi.org/10.1080/21663831.2016.1244116.

[66] J. Cavin, A. Ahmadiparidari, L. Majidi, A.S. Thind, S.N. Misal, A. Prajapati, Z. Hemmat, S. Rastegar, A. Beukelman, M.R. Singh, K.A. Unocic, A. Salehi-Khojin, R. Mishra, 2D high-entropy transition metal dichalcogenides for carbon dioxide electrocatalysis, Adv. Mater. 33 (31) (2021) 2100347, https://doi.org/10.1002/adma.202100347.

[67] Y. Ma, Y. Ma, S.L. Dreyer, Q. Wang, K. Wang, D. Goonetilleke, A. Omar, D. Mikhailova, H. Hahn, B. Breitung, T. Brezesinski, High-entropy metal–organic frameworks for highly reversible sodium storage, Adv. Mater. 33 (34) (2021) 101342, https://doi.org/10.1002/adma.202101342.

[68] Y. Huang Jr., J.W. Yeh, A. Chang-Mou Yang, High-entropy polymers: a new route of polymer mixing with suppressed phase separation, Mater 15 (2021) 100978, https://doi.org/10.1016/j.mtla.2020.100978.

[69] M. Cui, C. Yang, B. Li, Q. Dong, M. Wu, S. Hwang, H. Xie, X. Wang, G. Wang, L. Hu, High-entropy metal sulfide nanoparticles promise high-performance oxygen evolution reaction, Adv. Energy Mater. 11 (3) (2021) 2002887, https://doi.org/10.1002/aenm.202002887.

[70] A. Miura, S. Ishiyama, D. Kubo, N.C. Rosero-Navarro, K. Tadanaga, Synthesis and ionic conductivity of a high-entropy layered hydroxide, J. Ceram. Soc. Jpn. 128 (7) (2020) 336–339, https://doi.org/10.2109/jcersj2.20001.

[71] S.K. Nemani, B. Zhang, B.C. Wyatt, Z.D. Hood, S. Manna, R. Khaledialidusti, W. Hong, M.G. Sternberg, S.K.R.S. Sankaranarayanan, B. Anasori, High-Entropy 2D Carbide MXenes: TiVNbMoC3and TiVCrMoC3, ACS Nano 15 (8) (2021) 2815–12825, https://doi.org/10.1021/acsnano.1c02775.

[72] D. Berardan, A.K. Meena, S. Franger, C. Herrero, N. Dragoe, Controlled Jahn-Teller distortion in (MgCoNiCuZn)O-based high entropy oxides, J. Alloy. Compd. 704 (2017) 693–700, https://doi.org/10.1016/j.jallcom.2017.02.070.

[73] D. Bérardan, S. Franger, D. Dragoe, A.K. Meena, N. Dragoe, Colossal dielectric constant in high entropy oxides, Phys. Status Solidi Rapid Res. Lett. 10 (4) (2016) 328–333, https://doi.org/10.1002/pssr.201600043.

[74] S.H. Albedwawi, A. AlJaberi, G.N. Haidemenopoulos, K. Polychronopoulou, High entropy oxides-exploring a paradigm of promising catalysts: a review, Mater. Des. 202 (2021) 109534, https://doi.org/10.1016/j.matdes.2021.109534.

[75] K. Chen, X. Pei, L. Tang, H. Cheng, Z. Li, C. Li, X. Zhang, L. An, A five-component entropy-stabilized fluorite oxide, J. Eur. Ceram. Soc. 38 (11) (2018) 4161–4164, https://doi.org/10.1016/j.jeurceramsoc.2018.04.063.

[76] S.J. McCormack, A. Navrotsky, Thermodynamics of high entropy oxides, Acta Mater. 202 (2021) 1–21, https://doi.org/10.1016/j.actamat.2020.10.043.

[77] T. Li, Y. Yao, Z. Huang, P. Xie, Z. Liu, M. Yang, J. Gao, K. Zeng, A.H. Brozena, G. Pastel, M. Jiao, Q. Dong, J. Dai, S. Li, H. Zong, M. Chi, J. Luo, Y. Mo, G. Wang, C. Wang, R. Shahbazian-Yassar, L. Hu, Denary oxide nanoparticles as highly stable catalysts for methane combustion, Nat. Catal. 4 (1) (2021) 62–70, https://doi.org/10.1038/s41929-020-00554-1.

[78] H. Li, Y. Duan, Z. Zhao, X. Cheng, W. Bian, Z. Xiao, X. Wang, Atomic-scale storage mechanism in ultra-small size (FeCuCrMnNi)3O4/rGO with super-stable sodium storage and accelerated kinetics, Chem. Eng. J. 469 (2023) 143951, https://doi.org/10.1016/j.cej.2023.143951.

[79] B. Xiao, G. Wu, T. Wang, Z. Wei, Y. Sui, B. Shen, J. Qi, F. Wei, J. Zheng, High-entropy oxides as advanced anode materials for long-life lithium-ion Batteries, Nano Energy 95 (2022) 106962, https://doi.org/10.1016/j.nanoen.2022.106962.

[80] S. Nundy, D. Tatar, J. Kojčinović, H. Ullah, A. Ghosh, T.K. Mallick, R. Meinusch, B.M. Smarsly, A.A. Tahir, I. Djerdj, Bandgap Engineering in Novel Fluorite-Type Rare Earth High-Entropy Oxides (RE-HEOs) with computational and experimental validation for photocatalytic water splitting applications, Adv. Sustain. Syst. 6 (7) (2022) 2200067, https://doi.org/10.1002/adsu.202200067.

[81] P. Edalati, Q. Wang, H. Razavi-Khosroshahi, M. Fuji, T. Ishihara, K. Edalati, Photocatalytic hydrogen evolution on a high-entropy oxide, J. Mater. Chem. A 8 (7) (2020) 3814–3821, https://doi.org/10.1039/c9ta12846h.

[82] A. Sarkar, R. Kruk, H. Hahn, Magnetic properties of high entropy oxides, Dalton Trans. 50 (6) (2021) 1973–1982, https://doi.org/10.1039/d0dt04154h.

[83] U. Mizutani. Hume-Rothery Rules for Structurally Complex Alloy Phases, 2nd ed., CRC Press, Boca Raton, 2016 https://doi.org/10.1201/b10324.

[84] Y. Zhang, Y.J. Zhou, J.P. Lin, G.L. Chen, P.K. Liaw, Solid-solution phase formation rules for multi-component alloys, Adv. Eng. Mater. 10 (6) (2008) 534–538, https://doi.org/10.1002/adem.200700240.

[85] S. Guo, C.T. Liu, Phase stability in high entropy alloys: formation of solid-solution phase or amorphous phase, Prog. Nat. Sci. Mater. Int. 21 (6) (2011) 433–446, https://doi.org/10.1016/S1002-0071(12)60080-X.

[86] S. Fang, X. Xiao, L. Xia, W. Li, Y. Dong, Relationship between the widths of supercooled liquid regions and bond parameters of Mg-based bulk metallic glasses, J. Non-Cryst. Solids 321 (1-2) (2003) 120–125, https://doi.org/10.1016/S0022-3093(03)00155-8.

[87] Q.F. He, Y.F. Ye, Y. Yang, Formation of random solid solution in multicomponent alloys: from hume-rothery rules to entropic stabilization, J. Phase Equilibria Diffus. 38 (2017) 416–425, https://doi.org/10.1007/s11669-017-0560-9.

[88] K.Y. Tsai, M.H. Tsai, J.W. Yeh, Sluggish diffusion in Co–Cr–Fe–Mn–Ni high-entropy alloys, Acta Mater. 61 (13) (2013) 4887–4897, https://doi.org/10.1016/j.actamat.2013.04.058.

[89] K. Guruvidyathri, M. Vaidya, B.S. Murty, Challenges in design and development of high entropy alloys: A thermodynamic and kinetic perspective, Scr. Mater. 188 (2020) 37–43, https://doi.org/10.1016/j.scriptamat.2020.06.060.

[90] A. Sarkar, B. Breitung, H. Hahn, High entropy oxides: the role of entropy, enthalpy and synergy, Scr. Mater. 187 (2020) 43–48, https://doi.org/10.1016/j.scriptamat.2020.05.019.

[91] L. Tang, Z. Li, K. Chen, C. Li, X. Zhang, L. An, High-entropy oxides based on valence combinations: design and practice, J. Am. Ceram. Soc. 104 (5) (2021) 1953–1958, https://doi.org/10.1111/jace.17659.

[92] S. Jiang, T. Hu, J. Gild, N. Zhou, J. Nie, M. Qin, T. Harrington, K. Vecchio, J. Luo, A new class of high-entropy perovskite oxides, Scr. Mater. 142 (2018) 116–120, https://doi.org/10.1016/j.scriptamat.2017.08.040.

[93] J. Ma, K. Chen, C. Li, X. Zhang, L. An, High-entropy stoichiometric perovskite oxides based on valence combinations, Ceram. Int. 47 (17) (2021) 24348–24352, https://doi.org/10.1016/j.ceramint.2021.05.148.

[94] R. Djenadic, A. Sarkar, O. Clemens, C. Loho, M. Botros, V.S.K. Chakravadhanula, C. Kübel, S.S. Bhattacharya, A.S. Gandhi, H. Hahn, Multicomponent equiatomic rare earth oxides, Mater. Res. Lett. 5 (2) (2017) 102–109, https://doi.org/10.1080/21663831.2016.1220433.

[95] N.J. Usharani, R. Shringi, H. Sanghavi, S. Subramanian, S.S. Bhattacharya, Role of size, alio-/multi-valency and non-stoichiometry in the synthesis of phase-pure high entropy oxide (Co,Cu,Mg,Na,Ni,Zn)O, Dalton Trans. 49 (21) (2020) 7123–7132, https://doi.org/10.1039/d0dt00958j.

[96] M. Anandkumar, A. Lathe, A.M. Palve, A.S. Deshpande, Single-phase Gd0.2La0.2Ce0.2Hf0.2Zr0.2O2 and Gd0.2La0.2Y0.2Hf0.2Zr0.2O2 nanoparticles as efficient photocatalysts for the reduction of Cr(VI) and degradation of methylene blue dye, J. Alloy. Compd. 850 (2021) 156716, https://doi.org/10.1016/j.jallcom.2020.156716.

[97] F. Okejiri, Z. Zhang, J. Liu, M. Liu, S. Yang, S. Dai, Room-temperature synthesis of high-entropy perovskite oxide nanoparticle catalysts through ultrasonication-based method, ChemSusChem 13 (1) (2020) 111–115, https://doi.org/10.1002/cssc.201902705.

[98] F. Okejiri, J. Fan, Z. Huang, K.M. Siniard, M. Chi, F. Polo-Garzon, Z. Yang, S. Dai, Ultrasound-mediated synthesis of nanoporous fluorite-structured high-entropy oxides toward noble metal stabilization, iScience 25 (5) (2022) 104214, https://doi.org/10.1016/j.isci.2022.104214.

[99] S.L. Fereja, Z. Zhang, Z. Fang, J. Guo, X. Zhang, K. Liu, Z. Li, W. Chen, High-entropy oxide derived from metal-organic framework as a bifunctional electrocatalyst for efficient urea oxidation and oxygen evolution reactions, ACS Appl. Mater. Interfaces 14 (34) (2022) 38727–38738, https://doi.org/10.1021/acsami.2c09161.

[100] S. Aydinyan, H. Kirakosyan, A. Sargsyan, O. Volobujeva, S. Kharatyan, Solution combustion synthesis of MnFeCoNiCu and (MnFeCoNiCu)3O4 high entropy materials and sintering thereof, Ceram. Int. 48 (14) (2022) 20294–20305, https://doi.org/10.1016/j.ceramint.2022.03.310.

[101] M.V. Kante, M.L. Weber, S. Ni, I.C.G. van den Bosch, E. van der Minne, L. Heymann, L.J. Falling, N. Gauquelin, M. Tsvetanova, D.M. Cunha, G. Koster, F. Gunkel, S. Nemšák, H. Hahn, L. Velasco Estrada, C. Baeumer, A High-entropy oxide as high-activity electrocatalyst for water oxidation, ACS Nano 17 (6) (2023) 5329–5339, https://doi.org/10.1021/acsnano.2c08096.

[102] A.H. Phakatkar, M.T. Saray, M.G. Rasul, L.V. Sorokina, T.G. Ritter, T. Shokuhfar, R. Shahbazian-Yassar, Ultrafast synthesis of high entropy oxide nanoparticles by flame spray pyrolysis, Langmuir 37 (30) (2021) 9059–9068, https://doi.org/10.1021/acs.langmuir.1c01105.

[103] Y. Gu, A. Bao, X. Wang, Y. Chen, L. Dong, X. Liu, H. Pan, Y. Li, X. Qi, Engineering the oxygen vacancies of rocksalt-type high-entropy oxides for enhanced electrocatalysis, Nanoscale 14 (2) (2022) 515–524, https://doi.org/10.1039/D1NR07000B.

[104] H. Chen, J. Fu, P. Zhang, H. Peng, C.W. Abney, K. Jie, X. Liu, M. Chi, S. Dai, Entropy-stabilized metal oxide solid solutions as CO oxidation catalysts with high-temperature stability, J. Mater. Chem. A 6 (24) (2018) 1129–11133, https://doi.org/10.1039/c8ta01772g.

[105] S. Hou, X. Ma, Y. Shu, J. Bao, Q. Zhang, M. Chen, P. Zhang, S. Dai, Self-regeneration of supported transition metals by a high entropy-driven principle, Nat. Commun. 12 (1) (2021) 5917, https://doi.org/10.1038/s41467-021-26160-8.

[106] G. Wang, J. Qin, Y. Feng, B. Feng, S. Yang, Z. Wang, Y. Zhao, J. Wei, Sol-gel synthesis of spherical mesoporous high-entropy oxides, ACS Appl. Mater.

Interfaces 12 (40) (2020) 45155–45164, https://doi.org/10.1021/acsami.0c11899.
[107] D. Feng, Y. Dong, L. Zhang, X. Ge, W. Zhang, S. Dai, Z.A. Qiao, Holey lamellar high-entropy oxide as an ultra-high-activity heterogeneous catalyst for solvent-free aerobic oxidation of benzyl alcohol, Angew. Chem. Int. Ed. 59 (44) (2020) 19671–19677, https://doi.org/10.1002/anie.202004892.
[108] M. Einert, M. Mellin, N. Bahadorani, C. Dietz, S. Lauterbach, J.P. Hofmann, Mesoporous high-entropy oxide thin films: electrocatalytic water oxidation on high-surface-area spinel (Cr0.2Mn0.2Fe0.2Co0.2Ni0.2)3O4 Electrodes, ACS Appl. Energy Mater. 5 (1) (2022) 717–730, https://doi.org/10.1021/acsaem.1c03190.
[109] L. Li, X. Chang, X. Lin, Z.-J. Zhao, J. Gong, Theoretical insights into single-atom catalysts, Chem. Soc. Rev. 49 (22) (2020) 8156–8178, https://doi.org/10.1039/D0CS00795A.
[110] K.L. Svane, J. Rossmeisl, Theoretical optimization of compositions of high-entropy oxides for the oxygen evolution reaction, Angew. Chem. Int. Ed. 61 (19) (2022) e202201146, https://doi.org/10.1002/anie.202201146.
[111] K.K. Ghose, J.J. Brown, T.J. Frankcombe, A. Page, A. Bayon, Density functional theory modeling of critical properties of perovskite oxides for water splitting applications, WIREs Energy Environ. 12 (4) (2023) e476, https://doi.org/10.1002/wene.476.
[112] G. Anand, A.P. Wynn, C.M. Handley, C.L. Freeman, Phase stability and distortion in high-entropy oxides, Acta Mater. 146 (2018) 119–125, https://doi.org/10.1016/j.actamat.2017.12.037.
[113] T.X. Nguyen, Y.H. Su, J. Hattrick-Simpers, H. Joress, T. Nagata, K.S. Chang, S. Sarker, A. Mehta, J.M. Ting, Exploring the First High-Entropy Thin Film Libraries: Composition Spread-Controlled Crystalline Structure, ACS Comb. Sci. 22 (12) (2020) 858–866, https://doi.org/10.1021/acscombsci.0c00159.
[114] Z. Rak, C.M. Rost, M. Lim, P. Sarker, C. Toher, S. Curtarolo, J.P. Maria, D. W. Brenner, Charge compensation and electrostatic transferability in three entropy-stabilized oxides: Results from density functional theory calculations, J. Appl. Phys. 120 (9) (2016) 095105, https://doi.org/10.1063/1.4962135.
[115] A. Zywczak, P.A. Krawczyk, M. Jurczyszyn, J. Pawlak, W. Salamon, P. Baran, A. Kmita, Ł. Gondek, M. Sikora, C. Kapusta, T. Strączek, J. Wyrwa, High-entropy perovskites as multifunctional metal oxide semiconductors: synthesis and characterization of (Gd0.2Nd0.2La0.2Sm0.2Y0.2)CoO3, ACS Appl. Electron. Mater. 2 (10) (2020) 3211–3220, https://doi.org/10.1021/acsaelm.0c00559.
[116] Z. Rák, J.P. Maria, D.W. Brenner, Evidence for Jahn-Teller compression in the (Mg Co Ni Cu Zn)O entropy-stabilized oxide: A DFT study, Mater. Lett. 217 (2018) 300–303, https://doi.org/10.1016/j.matlet.2018.01.111.
[117] C.M. Rost, Z. Rak, D.W. Brenner, J.P. Maria, Local structure of the MgxNixCoxCuxZnxO(x=0.2) entropy-stabilized oxide: an EXAFS study, J. Am. Ceram. Soc. 100 (6) (2017) 2732–2738, https://doi.org/10.1111/jace.14756.
[118] R.R. Katzbaer, F.M. dos Santos Vieira, I. Dabo, Z. Mao, R.E. Schaak, Band gap narrowing in a high-entropy spinel oxide semiconductor for enhanced oxygen evolution catalysis, J. Am. Chem. Soc. 145 (12) (2023) 6753–6761, https://doi.org/10.1021/jacs.2c12887.
[119] S. Roy, Z. Li, Z. Chen, A.C. Mata, P. Kumar, S.C. Sarma, I.F. Teixeira, I.F. Silva, G. Gao, N.V. Tarakina, M.G. Kibria, C.V. Singh, J. Wu, P.M. Ajayan, Cooperative copper single-atom catalyst in 2D carbon nitride for enhanced CO2 electrolysis to methane, Adv. Mater. n/a (n/a) (2023) 2300713, https://doi.org/10.1002/adma.202300713.
[120] P. Du, R. Qi, Y. Zhang, Q. Gu, X. Xu, Y. Tan, X. Liu, A. Wang, B. Zhu, B. Yang, T. Zhang, Single-atom-driven dynamic carburization over Pd1–FeOx catalyst boosting CO2 conversion, Chem 8 (12) (2022) 3252–3262, https://doi.org/10.1016/j.chempr.2022.08.012.
[121] W.-Z. Yu, W.-W. Wang, S.-Q. Li, X.-P. Fu, X. Wang, K. Wu, R. Si, C. Ma, C.-J. Jia, C.-H. Yan, Construction of active site in a sintered copper–ceria nanorod catalyst, J. Am. Chem. Soc. 141 (44) (2019) 17548–17557, https://doi.org/10.1021/jacs.9b05419.
[122] P. Kumar, T.A. Al-Attas, J. Hu, M.G. Kibria, Single atom catalysts for selective methane oxidation to oxygenates, ACS Nano 16 (6) (2022) 8557–8618, https://doi.org/10.1021/acsnano.2c02464.
[123] M.D. Marcinkowski, S.F. Yuk, N. Doudin, R.S. Smith, M.-T. Nguyen, B.D. Kay, V.-A. Glezakou, R. Rousseau, Z. Dohnálek, Low-temperature oxidation of methanol to formaldehyde on a model single-atom catalyst: Pd Atoms on Fe3O4(001), ACS Catal. 9 (12) (2019) 10977–10982, https://doi.org/10.1021/acscatal.9b03891.
[124] R. Bliem, J.E.S. van der Hoeven, J. Hulva, J. Pavelec, O. Gamba, P.E. de Jongh, M. Schmid, P. Blaha, U. Diebold, G.S. Parkinson, Dual role of CO in the stability of subnano Pt clusters at the Fe3O4(001) surface, Proc. Natl. Acad. Sci. U. S. A. 113 (32) (2016) 8921–8926, https://doi.org/10.1073/pnas.1605649113.
[125] R. Bliem, R. Kosak, L. Perneczky, Z. Novotny, O. Gamba, D. Fobes, Z. Mao, M. Schmid, P. Blaha, U. Diebold, G.S. Parkinson, Cluster nucleation and growth from a highly supersaturated adatom phase: silver on magnetite, ACS Nano 8 (7) (2014) 7531–7537, https://doi.org/10.1021/nn502895s.
[126] Y. Chen, J. Lin, L. Li, B. Qiao, J. Liu, Y. Su, X. Wang, Identifying Size Effects of Pt as single atoms and nanoparticles supported on feox for the water-gas shift reaction, ACS Catal. 8 (2) (2018) 859–868, https://doi.org/10.1021/acscatal.7b02751.
[127] Z. Jiang, M. Jing, X. Feng, J. Xiong, C. He, M. Douthwaite, L. Zheng, W. Song, J. Liu, Z. Qu, Stabilizing platinum atoms on CeO2 oxygen vacancies by metal-support interaction induced interface distortion: mechanism and application, Appl. Catal. B 278 (2020) 119304, https://doi.org/10.1016/j.apcatb.2020.119304.
[128] L. Lei, H. Liu, Z. Wu, Z. Qin, G. Wang, J. Ma, L. Luo, W. Fan, J. Wang, Aerobic oxidation of alcohols over isolated single Au atoms supported on CeO2 nanorods: catalysis of interfacial [O–Ov–Ce–O–Au] Sites, ACS Appl. Nano Mater. 2 (8) (2019) 5214–5223, https://doi.org/10.1021/acsanm.9b01091.
[129] X. Tao, R. Long, D. Wu, Y. Hu, G. Qiu, Z. Qi, B. Li, R. Jiang, Y. Xiong, Anchoring Positively Charged Pd single atoms in ordered porous ceria to boost catalytic activity and stability in suzuki coupling reactions, Small 16 (43) (2020) 2001782, https://doi.org/10.1002/smll.202001782.
[130] Q. Gao, J. Hao, Y. Qiu, S. Hu, Z. Hu, Electronic and geometric factors affecting oxygen vacancy formation on CeO2(111) surfaces: a first-principles study from trivalent metal doping cases, Appl. Surf. Sci. 497 (2019) 143732, https://doi.org/10.1016/j.apsusc.2019.143732.
[131] A. Trovarelli, Catalytic Properties of Ceria and CeO2-Containing Materials, Catal. Rev. 38 (4) (1996) 439–520, https://doi.org/10.1080/01614949608006464.
[132] T. Montini, M. Melchionna, M. Monai, P. Fornasiero, Fundamentals and Catalytic Applications of CeO2-Based Materials, Chem. Rev. 116 (10) (2016) 5987–6041, https://doi.org/10.1021/acs.chemrev.5b00603.
[133] J. Lee, Y. Ryou, X. Chan, T.J. Kim, D.H. Kim, How Pt Interacts with CeO2 under the reducing and oxidizing environments at elevated temperature: the origin of improved thermal stability of Pt/CeO2 Compared to CeO2, J. Phys. Chem. C. 120 (45) (2016) 25870–25879, https://doi.org/10.1021/acs.jpcc.6b08656.
[134] V. Muravev, G. Spezzati, Y.-Q. Su, A. Parastaev, F.-K. Chiang, A. Longo, C. Escudero, N. Kosinov, E.J.M. Hensen, Interface dynamics of Pd–CeO2 single-atom catalysts during CO oxidation, Nat. Catal. 4 (6) (2021) 469–478, https://doi.org/10.1038/s41929-021-00621-1.
[135] H. Chen, W. Lin, Z. Zhang, K. Jie, D.R. Mullins, X. Sang, S.Z. Yang, C.J. Jafta, C. A. Bridges, X. Hu, R.R. Unocic, J. Fu, P. Zhang, S. Dai, Mechanochemical synthesis of high entropy oxide materials under ambient conditions: dispersion of catalysts via entropy maximization, ACS Mater. Lett. 1 (1) (2019) 83–88, https://doi.org/10.1021/acsmaterialslett.9b00064.
[136] Z. Jin, J. Lyu, K. Hu, Z. Chen, G. Xie, X. Liu, X. Lin, H.J. Qiu, Eight-component nanoporous high-entropy oxides with low ru contents as high-performance bifunctional catalysts in Zn-air batteries, Small 18 (12) (2022) 2107207, https://doi.org/10.1002/smll.202107207.
[137] C. Duan, X. Li, D. Wang, Z. Wang, H. Sun, R. Zheng, Y. Liu, Nanosized high entropy spinel oxide (FeCoNiCrMn)3O4 as a highly active and ultra-stable electrocatalyst for the oxygen evolution reaction, Sustain. Energy Fuels 6 (6) (2022) 1479–1488, https://doi.org/10.1039/D1SE02038B.
[138] J. Liu, C. Deng, X. Liu, S. Shao, P. Zheng, L. Chen, P. Wu, H. Li, H. Ji, W. Zhu, Single Mo atoms stabilized on high-entropy perovskite oxide: a frontier for aerobic oxidative desulfurization, Inorg. Chem. 62 (28) (2023) 11044–11055, https://doi.org/10.1021/acs.inorgchem.3c01085.
[139] H. Chen, Y. Sun, S. Yang, H. Wang, W. Dmowski, T. Egami, S. Dai, Self-regenerative noble metal catalysts supported on high-entropy oxides, Chem. Commun. 56 (95) (2020) 15056–15059, https://doi.org/10.1039/d0cc05860b.
[140] Y. Wei, Y. Zheng, Y. Hu, B. Huang, M. Sun, P. Da, P. Xi, C.H. Yan, Controlling the cation exsolution of perovskite to customize heterostructure active site for oxygen evolution reaction, ACS Appl. Mater. Interfaces 14 (22) (2022) 25638–25647, https://doi.org/10.1021/acsami.2c02861.
[141] S. Zhao, J. Lin, P. Wu, C. Ye, Y. Li, A. Li, X. Jin, Y. Zhao, G. Chen, Y. Qiu, D. Ye, A Hydrothermally Stable Single-Atom Catalyst of Pt Supported on High-Entropy Oxide/Al 2 O 3: structural optimization and enhanced catalytic activity, ACS Appl. Mater. Interfaces 13 (41) (2021) 48764–48773, https://doi.org/10.1021/acsami.1c14456.
[142] S. Zhu, Y. Chen, V. Somayaji, P. Novello, D. Chacko, F. Li, J. Liu, One-step synthesis of a high entropy oxide-supported rhodium catalyst for highly selective CO Production in CO2 hydrogenation, ACS Appl. Mater. Interfaces 15 (26) (2023) 31384–31392, https://doi.org/10.1021/acsami.3c02829.